Article:

Mo, P, Gao, X, Yang, W et al. (1 more author) (2020) A cavity expansion–based solution for interpretation of CPTu data in soils under partially drained conditions. International Journal for Numerical and Analytical Methods in Geomechanics, 44 (7). pp. 1053-1076. ISSN 0363-9061

https://doi.org/10.1002/nag.3050

A Cavity Expansion Based Solution for Interpretation of CPTu Data in Soils under Partially Drained Conditions

(Accepted version)

Pin-Qiang Mo[1], Xin-Wei Gao[2], Wenbo Yang[3*] and Hai-Sui Yu[4]

[1] Associate Research Scientist, State Key Laboratory for GeoMechanics and Deep Underground Engineering, School of Mechanics and Civil Engineering, China Univ. of Mining & Technology, Xuzhou, Jiangsu, 221116, China; Key Laboratory of Transportation Tunnel Engineering, (Southwest Jiaotong Univ.), Ministry of Education, Chengdu, 610031, China. E-mail: pinqiang.mo@cumt.edu.cn

[2] Postgraduate student, School of Mechanics and Civil Engineering, China Univ. of Mining & Technology, Xuzhou, Jiangsu, 221116, China. E-mail: 1273295465@qq.com

[3] Associate Professor, Key Laboratory of Transportation Tunnel Engineering (Southwest Jiaotong Univ.), Ministry of Education, Chengdu, 610031, China (**corresponding author**). E-mail: **yangwenbo1179@hotmail.com**

[4] Professor, Deputy Vice-Chancellor, School of Civil Engineering, Univ. of Leeds, Leeds LS2 9JT, U.K. E-mail: H.Yu@leeds.ac.uk

approx. 6000 words

22 Figures and 1 Table

ABSTRACT

A cavity expansion based solution is proposed in this paper for the interpretation of CPTu data under a partially drained condition. Variations of the normalized cone tip resistance, cone factor, and undrained-drained resistance ratio are examined with different initial specific volume and overconsolidation ratio, based on the exact solutions of both undrained and drained cavity expansion in CASM, which is a unified state parameter model for clay and sand. A drainage index is proposed to represent the partially drained condition, and the critical state after expansion and stress paths of cavity expansion are therefore predicted by estimating a virtual plastic region and assuming a drainage-index based mapping technique. The stress paths and distributions of stresses and specific volume are investigated for different values of drainage index, which are also related to the penetration velocity with comparisons of experimental data and numerical results. The subsequent consolidation after penetration is thus predicted with the assumption of constant deviatoric stress during dissipation of the excess pore pressure. Both spherical and cylindrical consolidations are compared for dissipation around the cone tip and the probe shaft, respectively. The effects of overconsolidation ratio on the stress paths and the distributions of excess pore pressure and specific volume are then thoroughly investigated. The proposed solution and the findings would contribute to the interpretation of CPTu tests under a random drained condition, as well as the analysis of pile installation and the subsequent consolidation.

Keywords: CPTu, cavity expansion method, partially drained condition, excess pore pressure

1 | INTRODUCTION

The cone penetration test has become one of the most popular and versatile in-situ soil testing methods, owing to its simplicity, economy efficiency and the obtained continuous records. The piezocone, usually terms as CPTu, was first invented in 1970s, and gradually becomes the standard configuration for cone penetrometers, which measures the pore water pressure typically behind the cone.[1] The penetration rate for a standard CPTu in practice is approximately 20mm/s, and the dissipation data can also be obtained during the pause of penetration. Together with the records of cone tip resistance, sleeve friction and pore pressure, the interpretation of CPTu data is applied for the determination of soil stratigraphy based on the Soil Behavior Type (SBT) charts, soil properties[1-3] and the equilibrium groundwater pressures, although many empirical correlations are usually employed. Additionally, the CPTu data is used for the assessment of liquefaction potential[4,5], and for the installation of driven piles[6,7] and suction caissons[8].

However, the understanding of penetration in soils under different drainage conditions is complicated by the formed large strains and high excess pore pressure, as well as the subsequent dissipation. Both consolidation coefficient of soils and penetration velocity have shown significant effects on the results of CPTu, based on field and laboratory tests, numerical simulation and analytical solutions. Moreover, the diameter of penetrometer affects the drainage distance that influences the profile of penetration-induced excess pore pressure and the following dissipation in reconsolidation. The penetrometer rate effect has been extensively reported by field experiments since the early penetration tests in clayey soils (e.g. Bemben and Myers[9]; Powell and Quarterman[10]; Lunne et al[11]; Schneider et al[12]; Kim[13]; Kim et al[14]). Experimental data was also provided by centrifuge tests and calibration chamber tests to identify the strong rate dependency of penetration resistance.[12,14,15-22] Drainage condition is dependent on both soil behaviour and penetration velocity, whereas the thresholds of penetration rate for undrained and drained conditions seem to vary with soil types.[23] With the increasingly developed numerical methods in geotechnical engineering applications, numerical simulations have shown their ability to provide insights into the penetration rate effect.[24-29] Owing to the complex process of penetration in soils, analytical methods for the interpretation of CPTu data are relatively limited. Randolph and Wroth[30] reported an analytical solution for radial consolidation of soil around a penetrometer with a logarithmic distribution of excess pore pressure, where rate effect was not included. Dislocation-based methods initially proposed by Elsworth[31] provided an alternative approximate method to accommodate the fluid pressure dissipation under partially drained conditions, while a pseudo-elastic material was assumed together with an incompressible flow field and a stress-decouple solution was employed to note the influence of soil rigidity to the penetration rate responses.[32]

As reported by Yu[33], cavity expansion methods in Geomaterials have been developed since 1950s[34,35], and their wide implications lead to the cavity expansion theory as a useful and simple tool for modelling many complex geotechnical problems, including in-situ soil testing (e.g. Ahmadi and Dariani[36]; Mo et al[37]; Vali et al[38]) and tunnelling (e.g. Yang et al[39]; Fang et al[40]; Mo and Yu[41]; Wang et al[42]). Numerous analytical and numerical solutions have been proposed using increasingly sophisticated constitutive soil models by applying the principles of continuum mechanics.[43-46] However, most of the existing solutions are developed with consideration of either fully undrained condition[46-50] or fully drained condition[43,51-53]. A more general situation for a geotechnical problem, e.g. cone penetration test, is under partially drained conditions, especially for tests within intermediate soils. Ceccato and Simonini[29] provided a numerical study of partially drained penetration and pore pressure dissipation in piezocone test, with a two-phase Material Point Method and the modified Cam-clay model.

Spherical cavity expansion in various drainage conditions was conducted by Suzuki and Lehane[28] using finite element method to evaluate the effect of soil permeability on CPT end resistance. Analytical solution of cavity expansion in terms of partially drained condition is currently not available in the literature.

This paper aims to propose a semi-analytical solution of cavity expansion for soils under a partially drained condition, to apply this solution for the interpretation of CPTu data with various penetration velocity, and to analyze the dissipation of excess pore pressure after penetration. The scenario of partially drained condition is taken as a general case between fully undrained and fully drained scenarios. With the provided stress-paths of both extreme conditions, a parameter of drainage index is proposed to indicate the partially drained condition within the stress fields. The relationship between the drainage index and the normalized penetration velocity is thus investigated to evaluate the drainage conditions during the cavity expansion and the cone penetration. With consideration of the penetration velocity, the penetration-induced changes of excess pore pressure, specific volume and their distributions at the surrounding soil are examined during and after penetration, as well as the effects of overconsolidation ratio.

2 | ANALYTICAL SOLUTIONS OF CAVITY EXPANSION AND THEIR IMPLICATIONS ON CPTU

It is widely accepted that critical state soil mechanics is an effective stress framework describing mechanical soil response[54-56], and serves as a milestone in the development of soil elasto-plastic models contributing to the further considerations of effects of anisotropy, fabric, and time-dependence, etc. (e.g. Nova and Wood[57]; Dafalias[58]; Kutter and Sathialingam[59]; Whittle[60]; Liu and Carter[61]). After reformulate the Cam-clay models in terms of the state parameter, a unified critical state soil model for both clay and sand, CASM (Clay And Sand Model), was proposed by Yu[62], together with the concept of spacing ratio and a non-associated flow rule. The soil model has been verified to generally capture the overall behaviour of sand clay under both drained and undrained conditions, while the simplicity of this model with easily measurable model constants contributes to the further extensions and convenient practical application (e.g. Sheng et al[63]; Khong[64]; Khalili et al[65]; Zhou and Ng[66]; Hu[67]).

Analytical solutions of cavity expansion in CASM have been proposed recently, including the undrained scenario[46] and the drained scenario[53]. The schematic of state parameter ξ in $\ln p' - v$ space is shown in Figure 1a, which is defined as the difference of specific volume between the current and critical state at the same mean effective stress: $\xi = v + \lambda \, ln \, p' - \Gamma$, where v is the specific volume, p' is mean effective stress and Γ is a critical-state parameter for specific volume at unit of stress. The state boundary surfaces is describes as: $(\eta/M)^n = 1 - \xi/\xi_R$, where η is the ratio of deviator stress and mean effective stress, M is the critical stress ratio; $\xi_R = (\lambda - \kappa) \, ln \, r^*$, indicating the reference state parameter, λ and κ are conventional critical state parameters; n is the stress-state coefficient and r^* is the spacing ratio. The shape of state boundary surfaces varies with n and r^*, as also presented in Figure 1b.

With the provided analytical solutions, the stress paths during cavity expansion can be calculated from an initial cavity size a_0 to an arbitrary cavity size a, as well as the stress/strain distributions after the process of expansion. Both spherical and cylindrical cavities have been considered within the solutions, together with the effective stress analysis for consideration of the generated excess pore water pressure. In terms of the scenario of fully undrained cavity, the volumetric strain remains zero for the soil around the cavity, and thus the excess pore pressure is generated in association with the equilibrium equation for total stresses (Figure 2a); whereas the stress paths of drained expansion are shown in Figure 2b, which also tend to approach to the critical state line with large expansion. More details on the derivations and calculation processes can be found in Mo and Yu[46,53].

Cavity expansion methods have been adopted for the interpretation of CPTu data, since 1940s.[68] For this study, the spherical cavity expansion analysis is used due to the reasonable analogy of soil deformation around the cone tip (e.g. Mo et al[69]). Considering the generated excess pore pressure during penetration, a relationship between the spherical cavity pressure and the cone tip resistance was provided by Suzuki and Lehane[28], as expressed by:

$$q_c = \sigma_{r,c} + \sqrt{3}(\sigma_{r,c} - \Delta u)\tan\delta \tag{1}$$

where $\sigma_{r,c}$ is the spherical cavity pressure at the cavity wall; δ is the interface friction angle, which can be assumed to be the constant volume friction angle of soil ϕ_{cs}; Δu is the excess pore pressure. Note that the correlation $q_c = \sigma_{r,c} \times (1 + \sqrt{3}\tan\phi_{cs})$ proposed by Randolph et al[70] could be recovered for fully drained tests of cohesionless soils.

3 | CPTU TESTS UNDER FULLY UNDRAINED AND DRAINED CONDITIONS

Unless stated otherwise, the soil model parameters are chosen as: $\Gamma = 2.759, \lambda = 0.161, \kappa = 0.062, \mu = 0.3, n = 2.0, r^* = 3.0, \phi_{cs} = 22.75°$ (i.e. $M = \frac{6\sin\phi_{cs}}{3-\sin\phi_{cs}} = 0.888$) for London clay; according to Yu[62], where Γ, λ, κ are the critical state parameters and μ is the Poisson's ratio. Spherical cavity expansion for $a/a_0 = 10$ is conducted for calculation of the limit cavity pressure, with the assumed initial water pressure $u_0 = 0$.

The normalized cone tip resistance is defined as:

$$Q = \frac{q_c - \sigma_{v0}}{\sigma'_{v0}} = \frac{q_{c,net}}{\sigma'_{v0}}\ , \tag{2}$$

where q_c is measured cone tip resistance, σ_{v0} and σ'_{v0} are the in-situ total and effective vertical stress respectively; $q_{c,net}$ is referred to as the net cone resistance, following Robertson and Caval[1]. For analysis of cavity expansion, the initial hydrostatic condition is assumed, thus the in-situ stress is denoted as: $p'_0 = \sigma_{v0} = \sigma'_{v0}$.

Fully Undrained Tests

The undrained tests of cavity expansion were carried out for numerical examples of London clay with various overconsolidation ratio (OCR), which were then correlated to the cone tip resistance of CPTu tests. For the proposed solutions in CASM, $R_0 = p'_{y0}/p'_0$ represents the isotropic overconsolidation ratio in terms of the mean effective stress, where p'_{y0} is the preconsolidation pressure; thus $OCR \approx R_0$. The series of tests include 8 groups with different value of R_0, which varies from 1 to 50. Each group was conducted with various initial specific volume v_0 , ranging between 1.4 and 2.6. Together with the soil parameters, the preconsolidation pressure, initial mean effective stress and initial stiffness G_0 could be calculated and estimated as:

$$\begin{aligned} p'_{y0} &= exp\left[\frac{\Gamma+(\lambda-\kappa)\, ln\, r^*+\lambda\ ln\, R_0-v_0}{\lambda}\right] \\ p'_0 &= \frac{p'_{y0}}{R_0} \\ G_0 &= \frac{(1+m)\,(1-2\,\mu)\,v_0\,p'_0}{2\,[1+(m-1)\,\mu]\,\kappa} \end{aligned} \quad , \tag{3}$$

where m is used to combine cylindrical and spherical analyses; i.e. $m = 1$ for cylindrical scenario, and $m = 2$ for spherical scenario. Therefore, v_0 ranging between 1.4 and 2.6 represents the magnitude of G_0/p'_0 varying from 10.4 to 19.4, for spherical cavity expansion.

Figure 3a presents the normalized cone tip resistance Q_{UD} (the subscript 'UD' indicates the undrained scenario) against the normalized stiffness (G_0/p'_0). Q_{UD} increases with both initial specific volume υ_0 (i.e. G_0/p'_0) and overconsolidation ratio R_0. Although Q_{UD} increases slightly with approximately 10% from $\upsilon_0 = 1.4$ to 2.6; while overconsolidation ratio shows a larger influence on the normalized cone tip resistance, that about 7.5 times larger Q_{UD} is obtained for $R_0 = 50$ compared to that of a normally consolidated soil test.

The cone factor for tests in clay under undrained conditions[6] is defined as:

$$N_c = \frac{q_c - \sigma_{v0}}{s_u} \quad , \tag{4}$$

where s_u is the undrained shear strength, defined as $s_u = 0.5\, M\, exp[(\Gamma - \upsilon_0)/\lambda]$ after Mo and Yu[46]. Note that the initial stress condition is assumed as hydrostatic, and K_0 effect is not included in this study, i.e. $\sigma_{v0} \approx p_0$. Figure 3b shows the relations between the cone factor N_c and the stiffness index (G_0/s_u). Linear correlations between N_c and $\ln(G_0/s_u)$ were proposed by previous researchers (e.g. Ladanyi and Johnson[71]; Vesic[72]; Yu[73]; van den Berg[74]; Lu[75]). For this test series of London clay, the following correlation with 97% of the coefficient of determination could be summarized as:

$$N_c = a' \times ln\frac{G_0}{s_u} + b' \qquad \text{where } a' = 1.32;\ b' = 3.75 \ . \tag{5}$$

Note that for soil with different overconsolidation ratio, the constants a' and b' vary slightly with R_0 for granular materials, as depicted in subplot of Figure 3b. Comparing with the relations proposed by Ladanyi and Johnson[71], Vesic[72] and Yu[73], the $N_c - \ln(G_0/s_u)$ correlation is found to vary with different soil types.

In terms of the undrained tests of cavity expansion, the excess pore pressure Δu is generated at the cavity wall; whereas for CPTu, pore pressure sensors are installed just behind the cone tip to measure the pore pressure u_2. The analysis in this study assumes that the excess pore pressure of cavity expansion is comparable to that measured in the corresponding penetration test (i.e. $\Delta u \approx u_2 - u_0 = u_2$). Robertson[76] and Robertson and Caval[1] reported a normalized CPT soil behaviour type (SBT) chart with $\mathrm{Q} - B_q$ for identification of soft, saturated fine grained soils, where B_q is the pore pressure ratio, defined as $B_q = \Delta u / q_{c,net} = \Delta u / (q_c - \sigma_{v0})$. Figure 4a presents the predicted $\mathrm{Q} - B_q$ data on the SBT chart, assuming the fully undrained cavity expansion for the CPTu tests. It shows that the soil behavior falls mainly within the zones of clay to silty clay, which matches to London clay. The predicted trends with increasing OCR agree well with the empirically summarized SBT chart, and the increase of Q and B_q with υ_0 is also observed.

To estimate the overconsolidation ratio based on the CPTu data, Mayne[77] proposed an analytical method based on Vesic's cavity expansion solution and the critical state soil mechanics, where OCR is related to a function of $(q_c - \Delta u)/\sigma'_{v0}$. Based on the solution of Mo and Yu[46], the correlation can therefore be modified and expressed as:

$$OCR = r^* \times \left[\frac{1}{\left(1+\sqrt{3}\tan\phi_{cs}\right)\left(1+\frac{m}{1+m}M\right)} \times \frac{q_c - \Delta u}{\sigma'_{v0}} \right]^{\frac{1}{\Lambda}} . \quad (6)$$

where $\Lambda = 1 - \kappa/\lambda$, representing the plastic volumetric strain potential; $0.7 < \Lambda < 0.8$ for many clays of low to medium sensitivity[78].

Figure 4b shows the curves of OCR with $(q_c - \Delta u)/\sigma'_{v0}$, for different parameter of the spacing ratio r^* ($r^* = 3.0$ for London clay in this study). Note that the curve of Equation 6 for $r^* = 2.0$ overlaps with that of Mayne[77] for the pore pressure behind the cone u_2 based on modified Cam-clay model, since the modified Cam-clay model is recovered by choosing $r^* = 2.0$ in conjunction with a suitable n value[62]. Therefore, the notable effect of spacing ratio on the relation between OCR and $(q_c - \Delta u)/\sigma'_{v0}$ is provided in Equation 6.

For in-situ tests, the undrained shear strength was predicted from the evaluated OCR. In this study, s_u can be expressed as a function of soil parameters, overconsolidation ratio, and initial stress state (Mo and Yu[46]), based on $s_u = q_{cs}/2$ (q_{cs} is the deviatoric stress at critical state):

$$\frac{s_u}{\sigma'_{v0}} = \frac{s_u}{p'_0} = \frac{M}{2}\left(\frac{OCR}{r^*}\right)^{\Lambda} , \quad (7)$$

The expression of $s_u/\sigma'_{v0} = 0.22 \times OCR^{0.8}$, can be recovered when setting $\Lambda = 0.8$, $r^* = 3.0$ and $\phi_{cs} = 26°$; which was proposed by Jamiolkowski et al[79], Ladd[80], and Ladd and DeGroot[81], based on their comprehensive experimental work at MIT.

Fully Drained Tests

Similar to undrained tests, the fully drained tests were also carried out for numerical examples of London clay using the corresponding cavity expansion solution (soil parameters were chosen the same as the undrained tests) with various overconsolidation ratio R_0 (1~50) and initial specific volume υ_0 (1.4~2.6). Correspondingly, Q_{DR} (the subscript 'DR' indicates the fully drained scenario) increases at approximately 30% from $\upsilon_0 = 1.4$ to 2.6, and Q_{DR} for $R_0 = 50$ is about 3.1 times the normally consolidated soil test, as shown in Figure 5a.

The cone factor of drained penetration tests, typically for cohesionless soils, is referred to as:

$$N_q = \frac{q_c}{\sigma'_{v0}} . \quad (8)$$

Figure 5b presents the relations of cone factor N_q with the normalized stiffness G_0/p'_0. The bearing capacity solution for CPT with an empirical shape factor was reported by Durgunoglu and Mitchell[82], which was not able to include the effects of soil stiffness and volume change:

$$N_q = 0.194 \times exp(7.63 \ tan\,\phi_{cs}) . \quad (9)$$

Based on the spherical cavity expansion approach, Vesic[72] related the cone factor with the friction angle ϕ_{cs} and the reduced rigidity index I_{rr}:

$$N_q = \left(\frac{1+2K_0}{3-\sin\phi_{cs}}\right) exp\left[\left(\frac{\pi}{2}-\phi_{cs}\right) tan\,\phi_{cs}\right] \times tan^2\left(\frac{\pi}{4}+\frac{\phi_{cs}}{2}\right)\,(I_{rr})^{\varrho}\ , \tag{10}$$

where K_0 is the in-situ stress ratio ($K_0 = 1$ in this study); $I_{rr} = I_s/(1 + I_s\,\varepsilon_v)$, in which the rigidity index $I_s = G_0/(p_0'\ tan\,\phi_{cs})$ and ε_v represents the average volumetric strain in the plastic region; constant $\varrho = 4\,sin\,\phi_{cs}\ [3(1 + sin\,\phi_{cs})]$. The curves based on Durgunoglu and Mitchell[82] and Vesic[72] are also shown in Figure 5b, with comparable predictions of the current results. However, the solution of this study has embedded the large strain analysis and the critical state concept within the exact solutions of cavity expansion. Additionally, the effects of overconsolidation ratio and initial specific volume are considered within the analysis, which indicates the novelties of the proposed solution.

Been and Jefferies[83] was the first to define the state parameter, which is then widely used for the interpretation of in-situ soil tests, especially for granular materials (e.g. Been et al[84,85]; Yu[86]; Schnaid and Yu[87]; Huang and Chuang[88]. The initial state parameter ξ_0 is related to the initial specific volume and the initial stress state, while the correlation between ξ_0 and overconsolidation ratio R_0 can be derived based on the schematic in Figure 1a, shown as follows:

$$\xi_0 = (\lambda - \kappa)\ln\left(\frac{r^*}{R_0}\right)\ . \tag{11}$$

Thus for a given initial specific volume, the value of initial state parameter decreases logarithmically with OCR. Figure 6 presents the variations of normalized penetration resistance Q_{DR} (subfigure a) and G_0/q_c (subfigure b) with the initial state parameter, for tests with different values of initial specific volume. From the results, higher normalized penetration resistance is observed for test with a lower value of ξ_0, which indicates that the initial soil state lies to the strong and dilating side of the critical state line in $\upsilon - \ln p'$ space. However, for tests with a constant value of OCR (i.e. constant ξ_0), both Q_{DR} and G_0/q_c increase with υ_0, while larger value of υ_0 represents a looser sample. Mathematically speaking, this phenomenon indicates that $d(Q_{DR})/d\upsilon_0 > 0$ and $d(G_0/q_c)/d\upsilon_0 > 0$ for soils with an identical state parameter. With the relation of $p'_0 = exp[(\xi_0 + \Gamma - \upsilon_0)/\lambda]$, the decreasing rate of p'_0 is obtained with $dp'_0/d\upsilon_0 = p'_0 \times (-1/\lambda)$. Therefore, the rates of penetration resistance q_c and Q_{DR} can be derives within the ranges, shown as follows:

$$\begin{aligned} &-q_c \times \frac{1}{\lambda} < \frac{dq_c}{d\upsilon_0} < -q_c \times \left(\frac{1}{\lambda} - \frac{1}{\upsilon_0}\right) < 0 \\ &0 < \frac{dQ_{DR}}{d\upsilon_0} < \frac{Q_{DR}+1}{\upsilon_0} \end{aligned} \quad . \tag{12}$$

These inequalities indicate that for a given initial state parameter, the penetration resistance q_c decreases with initial specific volume, since higher υ_0 gives larger initial void ratio but also smaller initial stress condition. On the other hand, the normalized penetration resistance Q_{DR} increases with υ_0, although larger void ratio represents a 'looser' sample.

Undrained-drained Resistance Ratio

The undrained-drained resistance ratio is defined as Q_{UD}/Q_{DR}, which represents the ratio of normalized penetration resistance under fully undrained and fully drained conditions. This series of tests show the decrease of the undrained-drained resistance ratio with the normalized stiffness, as presented in Figure 7. The overconsolidation ratio has a significant influence on the undrained-drained resistance ratio. It is seen that Q_{UD}/Q_{DR} increases exponentially with OCR, and the undrained resistance is normally smaller than the drained one for $R_0 < 50$. The results are also compared with previous research with normally consolidated clay (i.e. Yi et al[26] and Suzuki and Lehane[28]). Based on the large-displacement finite element analysis using a non-dilatant Drucker Prager model, Yi et al[26] proposed a linear relationship between Q_{DR}/Q_{UD} and G_0/p'_0, which is independent of friction angle. Despite of the differences on the ranges of normalized stiffness and constitutive models, the general trends from this study are in agreement with the predictions of Yi et al[26]. Numerical simulation of spherical cavity expansion in a non-linear Hardening Soil (HS) model[89] was conducted by Suzuki and Lehane[28], who provided a relationship between Q_{UD}/Q_{DR} and G_0/p'_0 with the effect of friction angle for normally consolidated kaolin clay. The relation agrees well with the result of this study for normally consolidated soil ($R_0 = 1$), as shown in Figure 7a. Moreover, to investigate the effect of friction angle ($\phi_{cs} = 18, 23, 27, 30, 35°$) for normally consolidated soil, Figure 7b provides the predicted curves of the undrained-drained resistance ratio, with comparisons of Yi et al[26] and Suzuki and Lehane[28], and the discrepancies are attributed to the differences on material parameters and state conditions. Relatively, the current analytical solutions show their ability for the prediction of the undrained-drained resistance ratio with considerations of friction angle, stiffness, stress state, and overconsolidation ratio.

4 | CPTU TESTS UNDER PARTIALLY DRAINED CONDITION

Penetration tests are normally conducted in a ground condition with mixed soil types, including clays, silts, and sands. The in-situ drainage condition is thus neither undrained nor drained. A partially drained condition leads to the consolidation effects during the process of penetration, which typically increases the penetration resistance; i.e. higher penetration resistance for fully drained tests has been observed in Figure 7. Therefore, the effects of partially drained conditions with soil permeability is required to be incorporated into the interpretation of CPTu data, with consideration of penetration velocity.

Effects of Penetration Rate

The normalized penetration velocity V for CPTu has been proposed by previous research (e.g. Finnie and Randolph[15]; Randolph and Hope[17]; Lee and Randolph[21]), which is defined as:

$$V = \frac{vD}{c_{vh}} , \tag{13}$$

in which v is cone penetration velocity, D is the penetrometer diameter, and c_{vh} indicates the coefficient of consolidation that governs the rate of pore pressure dissipation (the difference between horizontal and vertical consolidation is not considered in this study). Note that the normalized penetration velocity has included the effect of penetrometer diameter, as a larger penetrometer increases the drainage distance, and thus leads to a more undrained condition. According to Randolph[90], $V > 30{\sim}100$ typically represents the fully undrained penetration, whereas fully drained penetration occurs at $V < 0.03{\sim}0.01$.

To consider the effects of partial consolidation, the trend of normalized pore pressure ratio with variation of the normalized penetration velocity was proposed by DeJong and Randolph[91], which can be expressed as:

$$\frac{\Delta u}{\Delta u_{UD}} = 1 - \frac{1}{1+(V/V_{50})^{\varsigma}} , \tag{14}$$

where Δu is the excess pore pressure during penetration, Δu_{UD} is the excess pore pressure from the fully undrained penetration which serves as a reference; V_{50} represents the normalized velocity at which half of Δu_{UD} is generated by penetration; and ς is the maximum rate of change in $\Delta u/\Delta u_{UD}$ with V, numerically equals to $0.25\varsigma/V_{50}$ as noted by DeJong and Randolph[91] (the values of V_{50} and ς will be discussed later in this article). Similarly, the backbone-type of normalized function of penetration resistance[17,21,91] was defined as:

$$\frac{Q}{Q_{UD}} = 1 + \frac{Q_{DR}/Q_{UD}-1}{1+(V/V_{50})^{\varsigma}} \ , \tag{15}$$

where Q_{UD} and Q_{DR} indicate the normalized penetration resistance under undrained and fully drained conditions, respectively; 'V_{50}' and 'ς' were suggested to be the same parameters as Equation 14.

Cavity Expansion under a Partially Drained Condition

An example of spherical cavity expansion ($a/a_0 = 10$) with both undrained and drained conditions is provided as a reference in Figure 8, with soil parameters for lightly overconsolidated London clay; where original Cam-clay model is recovered by setting $r^* = 2.7183$ and $n = 1.0$, the overconsolidation ratio $R_0 = 1.5$, and the initial specific volume v_0 is 2.0. In Figure 8, the state 'A' represents the initial state before expansion with a hydrostatic condition; the elastic stage 'AB' appears at the early phase of expansion with small cavity deformation for both undrained and drained tests. As to the plastic stage, the effective stress path of undrained expansion follows the path of 'BC', while the total stress is developed following 'BD' (shown in Figure 8a; note that the initial pore pressure is neglected in this study). Excess pore pressure is thus indicated by the horizontal distance of 'CD' (Figure 8a). On the contrary, the stress path of the plastic stage for drained expansion tests goes through the rout of 'BE', with no excess pore pressure all along.

As both solutions are independent of time regarding to the quasi-static expansion, the soil consolidation during and after expansion was not included. The undrained scenario represents the extreme fast expansion in clayey soils with no pore pressure dissipation, whereas the fully drained scenario indicates the slow expansion in sandy or dry soils with instant pore pressure dissipation. However, the drainage condition of soils is normally neither fully undrained nor fully drained, and the cone penetration test in practical situations is also not extreme fast or slow. When the soil is set to be partially drained, the existing solution is not available for critical state soils, as well as the stress paths of cavity expansion.

Since the stress state after cavity expansion is between the states for undrained and drained tests, we could assume that the critical state for a certain drained condition locates at 'C'' on the critical state line in Figure 8, whereas '$C'D'$' represents the local excess pore pressure (Figure 8a). The total stress state 'D'' is then demonstrated here to be located at the line of 'DE', following the work of DeJong and Randolph (2012). At first, a drainage index 'χ' is introduced to represent the partially drained condition, as defined by:

$$\chi = \frac{1}{1+(V/V_{50})^{\varsigma}} \,, \tag{16}$$

which varies from 0 (fully undrained condition) to 1 (fully drained condition). In terms of the thresholds for fully undrained and fully drained conditions, it is easy to define with 5% of influence using the drainage index χ (i.e. $\chi_{UD} \leq 0.05$ represents fully undrained condition, and $\chi_{DR} \geq 0.95$ refers to fully drained condition). According to Equation 16, the thresholds of normalized penetration velocity are provided as $V_{UD} \geq 19^{1/\varsigma} \cdot V_{50}$ and $V_{DR} \leq 0.0526^{1/\varsigma} \cdot V_{50}$. Note that the same definition was referred to as a consolidation index by Lee and Randolph[21], regarding to the consolidation conditions. Combining Equations 2, 14 and 15 gives the following relations:

$$\chi = 1 - \frac{\Delta u}{\Delta u_{UD}} = \frac{Q - Q_{UD}}{Q_{DR} - Q_{UD}} = \frac{q_c - q_{c,UD}}{q_{c,DR} - q_{c,UD}} \ . \tag{17}$$

For the problems of CPTu, the drainage index also represents the ratio between drained and undrained penetration resistances at a corresponding partially drained condition. Relating the penetration resistance with the spherical cavity pressure following Suzuki and Lehane[28], we can have the ratio of cavity pressure at the cavity wall. Together with the total radial stress and the critical state relation, the following repressions can be obtained:

$$\chi = \frac{\sigma_{r,c} - \sigma_{r,c}|_{UD}}{\sigma_{r,c}|_{DR} - \sigma_{r,c}|_{UD}} = \frac{p\prime - p\prime_{UD}}{p\prime_{DR} - p\prime_{UD}} \ . \tag{18}$$

According to the effective mean stress and the excess pore pressure in Figure 8a, the geometry relations lead to: $\chi = C'C/EC = (CD - C'D')/CD$, thus $EC'/EC = C'D'/CD$ and 'D'' is located at the line of 'DE'. This phenomenon can also be verified by the numerical simulation of cavity expansion in both kaolin and Boston blue clay, conducted by Silva et al[24]. Therefore, the critical state is determined for a given drainage index; the effective and total stress paths for this partially drained test are noted as 'ABC'' and 'ABD'', respectively. A simple linear mapping technique is adopted to predict the stress path based on the two paths of both undrained and drained scenarios, which will be explained in the following section. This method could then be incorporated into the solutions of cavity expansion for the analysis of CPTu data interpretation in soils with partially drained conditions.

Results of CPTu Tests

The tests of fully undrained and drained cavity expansion, as shown in Figure 8, provide the distributions of stress and specific volume within both elastic and plastic zones. The stress paths show that the elastic stage overlaps for both undrained and drained tests, while the size of plastic zone is not the same. The normalized sizes of plastic zones for the above example tests are: $c_{UD}/a = 4.36$ and $c_{DR}/a = 3.21$ respectively, where c_{UD} is the size of cavity-expansion induced plastic region for undrained test and c_{DR} is the size of plastic region for fully drained test. Thus the size of plastic zone for a partially drained test is assumed with a linear relationship of drainage index, i.e. $c = c_{UD} + \chi \cdot (c_{DR} - c_{UD})$. A virtual radius of soil element in the plastic zone is scaled for the prediction of stress paths of partially drained test:

$$\begin{aligned} r'_{UD} - a &= (r_{UD} - a) \times \frac{c-a}{c_{UD}-a} \\ r'_{DR} - a &= (r_{DR} - a) \times \frac{c-a}{c_{DR}-a} \end{aligned} \quad . \tag{19}$$

where r_{UD} and r'_{UD} are the original and virtual radiuses of soil element in the plastic zone for undrained test, and r_{DR} and r'_{DR} are the corresponding original and virtual radiuses for fully drained test.

Therefore, the distributions of stress for both undrained and drained tests are obtained with the identical virtual radius r', and the stress path of partially drained test is predicted based on a simple mapping technique, according to Equations 16-18. For instance, the effective mean stress at r' is predicted as: $p'_{r\prime} = \chi \cdot \left(p'_{r',DR} - p'_{r',UD}\right) + p'_{r',UD}$. Figure 9a shows the stress paths in $p'/p'_{y0} - q/\left(M \cdot p'_{y0}\right)$ space under the conditions of drainage index $\chi = 0.3$ and 0.6, respectively. The critical excess pore pressure can be calculated based on Equation 14: $\Delta u/\Delta u_{UD} = 1 - \chi$, while the development of the excess pore pressure during expansion can also be deduced from the stress paths in Figure 9a. The critical state of specific volume can be derived based on

$$v_{cs} = v_0 - \lambda \left[\frac{\left(\frac{p'_{cs,DR}}{p'_{cs,UD}} - 1\right)}{\chi} + 1 \right] , \tag{20}$$

and the stress path in $\ln p' - v$ space as shown in Figure 9b is obtained after Mo and Yu[53], following the expression of:

$$\dot{v} = -\lambda \frac{\dot{p'}}{p'} - (\lambda - \kappa) \frac{\ln r^{*} \cdot n \cdot \eta^{n-1}}{M^{n}} \left(\frac{\dot{q}}{p'} - \frac{\eta \cdot \dot{p'}}{p'} \right) . \tag{21}$$

Correspondingly, the distributions of excess pore pressure and specific volume are presented against normalized radius (r/a) in Figure 10, for undrained ($\chi = 0$), drained ($\chi = 1$), and partially drained ($\chi = 0.3, 0.6$) tests.

According to the definition of drainage index, χ is related to the normalized penetration velocity using Equation 16. The parameters in Equations 14 and 16 are chosen as: $V_{50} = 3.0$ and $\varsigma = 1.0$, following DeJong and Randolph[91]. The values were obtained through reasonable agreement of $\Delta u/\Delta u_{UD} - V$ curve with experimental data for normally-consolidated kaolin clay with $Q_{DR}/Q_{UD} = 2.5$. The variations of parameters with the spread of published data were reported to be $0.3 < V_{50} < 8$ and $0.5 < \varsigma < 1.5$, and the characteristic curve with $V_{50} = 3.0$ and $\varsigma = 1.0$ was thus suggested due to the absence of sufficient site specific data[91]. To avoid obtaining Q_{DR} with impractically slow penetration tests in clay, the parameter values of V_{50} and ς were experimentally provided based on the $\Delta u/\Delta u_{UD} - V$ curves. Note that the relationships between the parameters (V_{50}, ς) and soil properties are not provided by the current solution.

Therefore, a certain penetration velocity corresponds to a drainage index χ, and the stress paths of spherical cavity expansion can be employed to predict the penetration resistance and induced excess pore pressure. Eventually, the relationships between penetration velocity and (1) excess pore pressure, (2) penetration resistance are then predicted through the semi-analytical solution, as shown in Figure 11.

The results of this study include two sets of tests in both lightly overconsolidated London clay and normally consolidated Speswhite kaolin clay, and their soil parameters and initial state conditions are listed in Table 1 according to Yu[93]. In addition, the predicted curves are also compared with the available data from the literature. Centrifuge tests in kaolin clay were performed by Randolph and Hope[17], Schneider et al[12] and Mahmoodzadeh and Randolph[92], and predicted curves agree well with the experimental data (in which $q_{c,DR}/q_{c,UD} = 2.6, 2.02, 2.5$ are used respectively). Numerical simulation of CPTu was carried out by Ceccato and Simonini[29], using modified Cam-clay model and the Darcy's permeability for pore pressure dissipation. The numerical results showed similar trends, while the parameters were suggested to be $V_{50} = 3.7, \varsigma = 1.1$ for the excess pore pressure ($\Delta u/\Delta u_{UD} - V$ curve in Figure 11a), and $V_{50} = 7.13, \varsigma = 0.95$ for the cone tip resistance ($\left(q_c - q_{c,UD}\right)/\left(q_{c,DR} - q_{c,UD}\right) - V$ curve in Figure 11b).

Table 1 Soil parameters and initial state conditions for London clay and Speswhite kaolin clay

	M	λ	κ	μ	Γ	n	r^*	R_0	v_0
London clay	0.89	0.161	0.062	0.3	2.759	1.0	2.718	1.5	2.0
Speswhite kaolin clay	0.86	0.19	0.03	0.3	3.056	2.0	2.718	1.0	2.0

Based on the definition of Robertson[76], the normalized pore pressure parameter B_q is presented in Figure 12, with variation of the normalized penetration velocity. Centrifuge data of piezocone tests in normally consolidated kaolin clay by Schneider et al[12] and Randolph and Hope[17], has been provided to show a good comparison with the calculation of lightly overconsolidated London clay, and slightly larger normalized pore pressure parameter is observed for calculated results of normally consolidated clay. Additionally, a couple-consolidation finite-element analysis with Drucker-Prager yield criterion, large deformation and finite sliding effects was reported by Yi et al[26], and the results with different normalized stiffness show comparative trends. Ceccato et al[94] proposed a two-phase material point method for piezocone penetration under different drainage conditions using modified Cam-clay model, and the results with different friction coefficient show similar value of B_q to the calculation of normally consolidated kaolin clay. Generally, the proposed semi-analytical solution of cavity expansion shows its ability for the predictions of both excess pore pressure and penetration resistance, with various normalized penetration velocity.

Correspondingly, the predictions of CPTu data in London clay with variation of penetration velocity are presented on the SBT chart (Figure 13), where the penetration velocity v increases from $0.001mm/s$ to $20mm/s$ (i.e. the standard velocity of CPTu tests). According to the normalization of penetration velocity (Equation 13), the penetrometer diameter is set as the standard cone with $D = 35.7mm$, and the magnitude of c_{vh} is estimated based on:

$$c_{vh} \approx \frac{2k' G_0 (1-\mu)}{(1-2\mu)\gamma_w} \ , \qquad (22)$$

where k' is the coefficient of permeability $= 1.5 \times 10^{-9} m/s$, $\gamma_w =$ unit weight of water; which lead to the normalized penetration velocity ranging from $V = 0.0278$ (fully drained) to $V = 556.9$ (fully undrained), respectively. The result shows that the normalized cone tip resistance decreases with the penetration velocity, although the higher excess pore pressure is generated around the cone tip for a fast penetration. In addition, Figure 14 shows the distributions of excess pore pressure and specific volume with the variation of penetration velocity, which also indicates the plastic zone increases with the penetration velocity for London clay with $R_0 = 1.5$.

5 | PORE PRESSURE DISSIPATION AFTER PENETRATION

Pore Pressure Dissipation

During the process of cone penetration under a partially drained condition, soil around the penetrometer is pushed and squeezed with partial consolidation. The generated distribution of the excess pore pressure is reduced compared to the undrained condition, and the pore pressure dissipation after penetration is also termed as the reconsolidation. In order to obtain the realistic dissipation curve, the pore water dissipation after penetration needs to start from the estimated excess pore pressure. The error introduced from the conventional normalization of dissipation data using the undrained assumption was discussed and corrected by DeJong and Randolph[91].

An ideal work-hardening soil model (i.e. modified Cam-clay) was adopted to perform the undrained cylindrical cavity expansion and the subsequent period of reconsolidation by Carter et al[95] and Randolph et al[96], where the numerical results showed that the deviatoric stress keeps almost constant during the reconsolidation. It is therefore convincing to assume that $\dot{q} = 0$ after penetration for CPTu tests. According to the equilibrium equation of cavity:

$$q = \sigma_r - \sigma_\theta = \frac{r}{m}\frac{\partial \sigma_r}{\partial r} \ , \tag{23}$$

it might be deduced that the distribution of total radial stress is not changed during the consolidation, which was also reported by Randolph and Wroth[30] although the elastic soil was used. Regarding to the definition of effective mean stress[46], the relation between $\dot{p}'$ and $\dot{\Delta u}$ can be obtained with elastic deformation assumption:

$$\dot{p}' = -\frac{1+\frac{m\nu}{1-\nu}}{1+m}\dot{\Delta u} \ . \tag{24}$$

Therefore, when the final state of soil around the cavity wall or cone tip after reconsolidation is noted as 'F'', the distance ratio of '$C'F'$' and '$D'F'$' in $p'/p'_{y0} - q/\left(M \cdot p'_{y0}\right)$ space is that: $C'F'/D'F' = [1 + (m-1)\nu]/[k - (2m+1)\nu]$, as represented in Figure 15a for both $\chi = 0$ and $\chi = 0.3$ in lightly overconsolidated London clay. In terms of the specific volume during pore pressure dissipation, the stress paths can be obtained by the integration of Equation 21, leading to the following repression:

$$\nu_{dissi} = \Gamma - \lambda \ln\left(p'_i\right) - \lambda \ln\left(\frac{p'_{dissi}}{p'_i}\right) - (\lambda - \kappa)\frac{\ln r^*}{M^n}\left(M \cdot p'_i\right)^n \left(\frac{1}{{p'_{dissi}}^n} - \frac{1}{{p'_i}^n}\right) . \tag{25}$$

The stress paths shown in Figure 15 can also be verified with the results of Carter et al[95], Silva et al[24], and DeJong and Randolph[91], showing that the changes of deviatoric stress during the reconsolidation are arguably negligible.

The dissipation of pore water around the penetrometer is taken as a radial consolidation problem assuming that soil deforms elastically, following Randolph et al[96]. However, as the penetration is treated as spherical cavity expansion around the cone tip and cylindrical cavity expansion around the penetrometer shaft, it seems more reasonable to assume that both spherical and cylindrical scenarios of radial consolidation are applied for the prediction of pore pressure dissipation after penetration. When soil is assumed to be distorted by spherical cavity expansion due to the pass-by of penetrometer, the horizontal pore pressure dissipation is taken as cylindrical for soil around the probe shaft during the subsequent consolidation after penetration. Therefore, according to Terzaghi's one-dimensional consolidation equation with respect to the Darcy's law, the governing equation of radial consolidation is provided as follows:

$$c_{vh} \cdot \left[\frac{\partial^2 \Delta u}{\partial r^2} + \frac{m}{r}\frac{\partial \Delta u}{\partial r}\right] = \frac{\partial \Delta u}{\partial t} . \tag{26}$$

The normalized reconsolidation time for any particular degree of consolidation is defined by Teh and Houlsby[97], as $T^* = (c_{vh} \cdot t)/\left(a^2 \cdot \sqrt{I_r}\right)$, where a is the probe/cavity radius and $I_r = G_0/s_u$ is the stiffness index. With the variable separate method, the distributions of pore pressure before and after reconsolidation are shown in Figure 16a for $\chi = 0.3$. Note that the spherical radial consolidation was adopted for the dissipation around the cone tip. It can be found that the pore pressure in the plastic zone dissipates with time and also extends to the elastic region. Correspondingly, the distributions of specific volume before and after reconsolidation are predicted based on Equation 25, as presented in Figure 16b, for both $\chi = 0$ and $\chi = 0.3$. Compared to the drained test $\chi = 1$, the porosity of soil closed to the cone tip decreases with the drainage index, even after reconsolidation.

Comparisons of Spherical and Cylindrical Scenarios

The excess pore pressure dissipation around a driven pile is normally considered as radial consolidation in a cylindrical scenario (e.g. Randolph and Wroth[30]; Li et al[98]). While spherical cavity expansion, assumed for penetration of the cone tip, generates the excess pore pressure in associate with the dissipation under a spherical scenario, the stage of reconsolidation for soil around the shaft is treated as the dissipation around a cylindrical cavity. Therefore, additional to the typical pore pressure transducers (PPTs) around the cone shoulder, it would be useful to install new PPTs at the probe shaft with some distance to the cone tip, and records of both spherical and cylindrical dissipations could mutually confirm the interpretations. Further study is required to validate this suggestion with more practical evidences. Thus the comparisons of spherical and cylindrical scenarios are provided in this section. Figure 17 shows the stress paths during penetration and the subsequent consolidation, with identical initial conditions and soil parameters. The effective stress paths seem to be close during the cavity expansion, while about 13% larger value of effective stress is achieved by spherical scenario and the excess pore pressure is approximate 1.5 times the cylindrical scenario, at the critical state after expansion. The results of reconsolidation show that the spherical scenario gains more radial stress during pore pressure dissipation, and the specific volume of cylindrical scenario is relatively higher after the subsequent consolidation. However, the influence zone in the surrounding soil appears to be larger for cylindrical scenario, as can be observed from the distributions of specific volume before and after reconsolidation for both spherical and cylindrical scenarios in Figure 18a. In addition, the changes of pore pressure and radial stress with reconsolidation time are presented in Figure 18b, where Δu_i indicates the initial value of pore pressure after cavity expansion and $\sigma'_{r,f}$ indicates the final value of effective radial stress after reconsolidation, respectively. It is found that both dissipation of excess pore pressure and increase of effective radial stress start earlier for spherical scenario. Li et al[98] provided centrifuge data on the increase of end bearing resistance of a driven pile with reconsolidation time, which shows a good agreement with the increase of σ'_r for spherical scenario.

Figure 19a provides the dissipation curves with different values of drainage index for both spherical and cylindrical scenarios. Larger value of χ indicates higher drainage condition with lower cavity-expansion induced excess pore water pressure. Cylindrical scenario appears to have lower Δu_i after cavity expansion, and cylindrical dissipation is typically slower, owing to the undrained condition along the plane-strain axis. The variations of normalized effective radial stress are shown in Figure 19b, validating the increase of effective stress during reconsolidation.

Effects of Overconsolidation Ratio

The overconsolidation ratio has shown its influences on the results of both undrained and drained tests of cavity expansion[46,53]. The effects of R_0 on cavity expansion and the subsequent consolidation are presented in this section, for a partially drained condition. The distributions of excess pore pressure are provided after penetration ($t = 0$) in Figure 20a, showing that the normalized excess pore pressure at the cavity wall increases with overconsolidation ratio, but the influence zone or plastic region is smaller for more heavily overconsolidated soil. It is also noted that slightly negative pore pressure appears at $2.0 < r/a < 2.5$ for test with $R_0 = 10$. Correspondingly, the distributions of specific volume is shown in Figure 20b, and the porosity of soil adjacent to the cone tip is higher for tests with larger value of R_0.

Figure 21 shows the stress paths of cavity expansion and the subsequent consolidation for tests with variation of R_0 and a given drainage index of $\chi = 0.3$. The initial condition with identical value of specific volume represents the variation of the initial state parameter ξ_0. The overconsolidation ratio shows a significant influence on the stress paths during cavity expansion, whereas the critical state is achieved with the decrease of stresses against R_0. Although the normalized pore pressure at the cavity wall increases with the overconsolidation ratio, the dissipation of Δu appears to be more significant for normally-consolidated soils with a higher increase of effective mean stress. On the other hand, the porosity of soil after both expansion and reconsolidation increases with the magnitude of overconsolidation ratio, as shown in Figure 21b.

The dissipation curves against normalized time T^* with variation of R_0 and a given drainage index of $\chi = 0.3$ are provided in Figure 22a, as well as the increases of radial stress. Larger R_0 value generates higher excess pore pressure, and the normalized effective stress increases in a smaller ratio. After reconsolidation, distribution curves of specific volume tend to move downwards with pore pressure dissipation, as depicted in Figure 22b.

Due to the complexity of the analytical solutions using CASM, it is difficult to propose the explicit relations with soil parameters for the evaluated values. However, the analysis for various soil properties and initial conditions can be provided efficiently, which could also contribute to the engineering practice effectively. Note that, besides of the consolidation effect during penetration, the viscous effect[99] would result in the increase of penetration resistance for a high penetration velocity, which is out of scope of this study. In addition, the dilatory dissipation[100], caused by the decay in time and dilation of soils, is also not considered. Further investigation is still required to study the effects of overconsolidation, initial state parameter, spacing ratio, and stress state coefficient on the stress paths, the changes of excess pore pressure and cone penetration resistance under a partially drained condition. In addition, the proposed solution serves as a benchmark for a related numerical simulation, and could also be applied to analyze problems of pile foundations and tunnelling.

6 | CONCLUSIONS

A cavity expansion based solution for the interpretation of CPTu data has been proposed under a partially drained condition. Exact solutions of both undrained and drained cavity expansion in CASM were combined as two extremes of penetration tests with a partially drained condition. The variations of the normalized cone tip resistance and the cone factor were examined with different initial specific volume and overconsolidation ratio for both undrained and drained tests; whereas the prediction of the undrained-drained resistance ratio considered the effects of friction angle, stress state, and overconsolidation ratio, in associate with good comparisons to the existing research. A drainage index was proposed to represent the partially drained condition, and the critical state of cavity expansion for penetration tests was verified for both effective stresses and the excess pore pressure. A virtual radius of the surrounding soil for undrained and drained tests was introduced according to the estimated plastic region, and the stress paths and the distributions of stresses and specific volume could thus be deduced for different values of drainage index, which was also related to the penetration velocity with validation by experimental data and numerical results. The subsequent consolidation after penetration was also predicted with the assumption of constant deviatoric stress during dissipation of the excess pore pressure. Both spherical and cylindrical consolidation were considered for dissipation around the cone tip and the probe shaft, respectively. In addition, the effects of overconsolidation ratio on the stress paths and the distributions of excess pore pressure and specific volume were investigated. The proposed semi-analytical solution contributes to the understanding of the CPTu tests under a partially drained condition, but also serves as an effective method for the evaluation of installation and reconsolidation of pile foundations and tunnelling.

ACKNOWLEDGMENTS

The authors would like to acknowledge financial supports from the Foundation of Key Laboratory of Transportation Tunnel Engineering (Southwest Jiaotong University), Ministry of Education (no. TTE2017-04), National Natural Science Foundation of China (no. 51908546), Natural Science Foundation of Jiangsu Province (no. BK20170279), the Independent Innovation Project for Double First-level Construction (China University of Mining and Technology) (2018ZZCX04), China Postdoctoral Science Foundation (no. 2017M621866), and Jiangsu Planned Projects for Postdoctoral Research Funds (no. 1701196B).

NOTATION

The following symbols are used in this paper:

$a_0, a =$ initial and current cavity radius;

$B_q =$ pore pressure ratio;

$c =$ size of plastic zone;

$c_{vh} =$ coefficient of consolidation;

$D =$ penetrometer diameter;

$K_0 =$ in-situ stress ratio;

$m =$ parameter for combining cylindrical and spherical scenarios;

$n =$ stress-state coefficient;

$N_c =$ cone factor for clay under undrained conditions;

$N_q =$ cone factor of drained penetration tests;

$OCR =$ overconsolidation ratio;

$p' =$ mean effective stress;

$p'_{y0} =$ preconsolidation pressure;

$q_c =$ cone tip resistance;

$q_{c,net} =$ net cone tip resistance;

$Q =$ normalized cone tip resistance;

$r^* =$ spacing ratio;

$r, r' =$ radius and virtual radius;

$R_0 =$ isotropic overconsolidation ratio;

$s_u =$ undrained shear strength;

$u_0 =$ initial water pressure;

$u_1, u_2 =$ pore pressure at cone face and behind the cone;

$v =$ cone penetration velocity;

$V =$ normalized penetration velocity;

$\gamma_w =$ unit weight of water;

$\Gamma, \lambda, \kappa, M =$ critical state parameters;

$\delta =$ interface friction angle;

$\Delta u =$ excess pore pressure;

k' = coefficient of permeability;

μ = Poisson's ratio;

ν, ν_0 = specific volume and initial specific volume;

ξ, ξ_0, ξ_R = state parameter, initial state parameter, reference state parameter;

$\sigma_{r,c}$ = cavity pressure;

$\sigma_{v0}, \sigma'_{v0}$ = in-situ total and effective vertical stress;

ϕ_{cs} = constant volume friction angle of soil; and

χ = drainage index.

REFERENCE

1. Robertson PK, Caval KL. Guide to Cone Penetration Testing for Geotechnical Engineering 4th Edition. Gredd Drilling & Testing, Inc., California; 2010.

2. Jamiolkowski M, Lo Presti DCF, Manassero M. Evaluation of relative density and shear strength of sands from CPT and DMT. *Soil Behavior and Soft Ground Construction*. 2003;7(119):201-238.

3. Kim C, Kim S, Lee J. Estimating clay undrained shear strength using CPTu results. *Proceedings of the Institution of Civil Engineers-Geotechnical Engineering*. 2009;162(2):119-127.

4. Moss RES, Seed RB, Kayen RE, Stewart JP, Kiureghian AD, Cetin KO. CPT-based probabilistic and deterministic assessment of in situ seismic soil liquefaction potential. *J Geotech Geoenviron Eng*. 2006;132(8):1032-1051.

5. Shuttle DA, Cunning J. Liquefaction potential of silts from CPTu. *Can Geotech J*. 2007;44(1):1-19.

6. Robertson PK, Campanella RG. Axial capacity of driven piles in deltaic soils using CPT. *Penetration Testing 1988*, ISOPT-1, pp. 919-928.

7. White DJ, Bolton MD. Comparing CPT and pile base resistance in sand. *Proceedings of the Institution of Civil Engineers-Geotechnical Engineering*. 2005;158(1):3-14.

8. Senders M, Randolph MF. CPT-Based Method for the Installation of Suction Caissons in Sand. *J Geotech Geoenviron Eng*. 2009;135(1):14-25.

9. Bemben SM, Myers DA. The influence of rate of penetration on static cone resistance in Connecticut river valley varved clay. *The European Symposium on Penetration Testing (ESOPT)*, Stockholm, National Swedish Building Research, 1974, Vol. 2, 33-34.

10. Powell JJM, Quarterman RST. The interpretation of cone penetration tests in clays, with particular reference to rate effects. *Proc Int Sym On Penetration Testing*, Orlando, 1988, pp. 903-909.

11. Lunne T, Robertson P, Powell J. Cone penetration testing in geotechnical practice. Blackie Academic & Professional, London; 1997.

12. Schneider JA, Lehane BM, Schnaid F. Velocity effects on piezocone measurements in normally and over consolidated clays. *Int J Phys Model Geotech*. 2007;7(2):23-34.

13. Kim K. Cone penetration test in clayey soil: Rate effect and application to pile shaft resistance calculations. PhD Thesis, Purdue University, Indiana, United States; 2005.

14. Kim K, Prezzi M, Salgado R, Lee W. Effect of penetration rate on cone penetration resistance in saturated clayey soils. *J Geotech Geoenviron Eng*. 2008;134(8):1142-1153.

15. Finnie IMS, Randolph MF. Punch-through and liquefaction induced failure of shallow foundations on calcareous sediments. *Proceedings of the 17th international conference on the behaviour of offshore structures (BOSS' 94)*. Pergamon Press; 1994, pp. 217-30.

16. House AR, Oliveira JRMS, Randolph MF. Evaluating the coefficient of consolidation using penetration tests. *Int J Phys Model Geotech*. 2001;1(3):17-25.

17. Randolph MF, Hope SF. Effect of cone velocity on cone resistance and excess pore pressures. *Proceedings of the International Symposium on Engineering Practice and Performance of Soft Deposits (IS-OSAKA 2004).* Yodogawa Kogisha; 2004, pp. 147-152.

18. Chung SF, Randolph MF. Penetration resistance in soft clay for different shaped penetrometers. *2nd International Conference on Geotechnical and Geophysical Site Characterization*, Porto, 2004, pp. 671-677.

19. Lehane BM, O'Loughlin CD, Gaudin C, Randolph MF. Rate effects on penetrometer resistance in kaolin. *Géotechnique*, 2009;59(1):41-52.

20. Jaeger RA, DeJong JT, Boulanger RW, Low HE, Randolph MF. Variable penetration rate CPT in an intermediate soil. *2nd International Symposium on Cone Penetration Testing*, Huntington Beach, 2010.

21. Lee J, Randolph MF. Penetrometer based assessment of spudcan penetration resistance. *J Geotech Geoenviron Eng*. 2011;137(6):587-596.

22. Suzuki Y, Lehane BM. Field observations of CPT penetration rate effects in Burswood clay. *Proceedings of the 3rd international symposium on cone penetration testing (CPT14).* Las Vegas, Nevada. 2014, pp. 403-410.

23. Suzuki Y. Investigation and interpretation of cone penetration rate effects. PhD Thesis, University of Western Australia; 2015.

24. Silva MF, White DJ, Bolton MD. An analytical study of the effect of penetration rate on piezocone tests in clay. *Int J Numer Anal Methods Geomech*. 2006;30(6):501-27.

25. Jaeger RA. Numerical and Experimental Study on Cone Penetration in Sands and Intermediate Soils. PhD Thesis, University of California Davis, Davis, California, United States; 2012.

26. Yi JT, Goh SH, Lee FH, Randolph MF A numerical study of cone penetration in fine-grained soils allowing for consolidation effects. *Géotechnique*. 2012;62(8):707-19.

27. Sheng D, Kelly R, Pineda J, Bates L. Numerical study of rate effects in cone penetration test. *Proceedings of the 3rd international symposium on cone penetration testing (CPT14)*, Las Vegas, Nevada. 2014, pp. 419-428.

28. Suzuki Y, Lehane BM.. Analysis of CPT end resistance at variable penetration rates using the spherical cavity expansion method in normally consolidated soils. *Computers and Geotechnics*. 2015;65:141-152.

29. Ceccato F, Simonini P. Numerical study of partially drained penetration and pore pressure dissipation in piezocone test. *Acta Geotechnica*. 2017;12(1):195-209.

30. Randolph MF, Wroth CP. An analytical solution for the consolidation around a driven pile. *Int J Numer Anal Methods Geomech*. 1979;3(3):217-229.

31. Elsworth D. Dislocation analysis of penetration in saturated porous media. *Journal of Engineering Mechanics*. 1991;117(2):391-408.

32. Elsworth D. The evaluation of pore pressure fields around standard and ball penetrometers: influence of penetration rate. *Int J Numer Anal Methods Geomech*. 2013;37: 2135-2153.

33. Yu HS. Cavity Expansion Methods in Geomechanics. Kluwer Academic Publishers, The Netherlands; 2000.

34. Gibson RE. Correspondence. *J. Inst. Civ. Engrs.*, 1950;34:382-383.

35. Gibson RE, Anderson W. In situ measurement of soil properties with the pressuremeter. *Civil Engineering and Public Review*. 1961;56(658):615-618.

36. Ahmadi MM, Dariani AAG. Cone penetration test in sand: A numerical-analytical approach. *Computers and Geotechnics*. 2017;90:176-189.

37. Mo PQ, Marshall AM, Yu HS. Interpretation of Cone Penetration Test Data in Layered Soils Using Cavity Expansion Analysis. *J Geotech Geoenviron Eng*. 2017;143(1): 04016084.

38. Vali R, Khotnehsara EM, Saberian M, Li J, Mehrinejad M, Jahandari S. A three-dimensional numerical comparison of bearing capacity and settlement of tapered and under-reamed piles. *International Journal of Geotechnical Engineering*. 2017;1-13. DOI: 10.1080/19386362.2017.1336586.

39. Yang W, Hussein MFM, Marshall AM. Centrifuge and numerical modelling of ground-borne vibration from an underground tunnel. *Soil Dynamics and Earthquake Engineering*. 2013;51:23-34.

40. Fang Y, Xu C, Cui G, Kenneally B. Scale model test of highway tunnel construction underlying mined-out thin coal seam. *Tunnelling and Underground Space Technology*. 2016;56:105-116.

41. Mo PQ, Yu HS. Undrained Cavity Contraction Analysis for Prediction of Soil Behaviour around Tunnels. *International Journal of Geomechanics (ASCE)*. 2017;17(5):04016121.

42. Wang F, Wang M, Huo J. The effects of the passive fire protection layer on the behavior of concrete tunnel linings: A field fire testing study. *Tunnelling and Underground Space Technology*. 2017;69:162-170.

43. Yu HS, Houlsby GT. Finite cavity expansion in dilatant soils: loading Analysis. *Géotechnique*. 1991;41(2):173–183.

44. Salgado R, Mitchell JK, Jamiolkowski M. Cavity expansion and penetration resistance in sand. *J Geotech Geoenviron Eng*. 1997;123(4):344-354.

45. Russell AR, Khalili N. On the problem of cavity expansion in unsaturated soils. *Computational Mechanics*. 2006;37(4):311-330.

46. Mo PQ, Yu HS. Undrained cavity expansion analysis with a unified state parameter model for clay and sand. *Géotechnique*. 2017;67(6): 503-515.

47. Davis RO, Scott RF, Mullenger G. Rapid expansion of a cylindrical cavity in a rate-type soil. *Int J Numer Anal Methods Geomech*. 1984;8(2):125-140.

48. Collins IF, Yu HS. Undrained cavity expansions in critical state soils. *Int J Numer Anal Methods Geomech*. 1996;20(7):489-516.

49. Cao LF, Teh CI, Chang MF. Undrained cavity expansion in modified cam clay I: Theoretical analysis. *Géotechnique*. 2001;51(4):323-334.

50. Chen SL, Abousleiman YN. Exact undrained elasto-plastic solution for cylindrical cavity expansion in modified cam clay soil. *Géotechnique*. 2012;62(5):447-456.

51. Collins IF, Pender MJ, Wang Y. Cavity expansion in sands under drained loading conditions. *Int J Numer Anal Methods Geomech*. 1992;16(1):3-23.

52. Chen SL, Abousleiman YN. Exact drained solution for cylindrical cavity expansion in modified cam clay soil. *Géotechnique*. 2013;63(6):510-517.

53. Mo PQ, Yu HS. Drained cavity expansion analysis with a unified state parameter model for clay and sand. *Can Geotech J*. 2018;55(7):1029-1040.

54. Roscoe KH, Schofield AN, Wroth CP. On the yielding of soils. *Géotechnique*. 1958;8(1):22-53.

55. Roscoe KH, Burland JB. On the generalized stress-strain behaviour of wet clay. in: Heymann, G., Leckie, F.A. (Eds.), Engineering Plasticity. Cambridge University Press, London, 1968, pp. 535-609.

56. Schofield AN, Wroth P. Critical state soil mechanics. McGraw-Hill, London; 1968.

57. Nova R, Wood DM. A constitutive model for sand in triaxial compression. *Int J Numer Anal Methods Geomech*. 1979;3(3):255-278.

58. Dafalias YF. An anisotropic critical state soil plasticity model. *Mechanics Research Communications*. 1986;13(6):341-347.

59. Kutter B, Sathialingam N. Elastic-viscoplastic modelling of the rate-dependent behaviour of clays. *Géotechnique*. 1992;42(3):427-441.

60. Whittle AJ. Evaluation of a constitutive model for overconsolidated clays. *Géotechnique*. 1993;43(2):289-313.

61. Liu MD, Carter JP. A structured Cam Clay model. *Canadian Geotechnical Journal*. 2002;39(6):1313-1332.

62. Yu HS. CASM: A unified state parameter model for clay and sand. *Int J Numer Ana. Methods Geomech*. 1998;22(8):621-653.

63. Sheng D, Sloan SW, Yu HS. Aspects of finite element implementation of critical state models. *Computational mechanics*, 2000;26(2):185-196.

64. Khong CD. Development and numerical evaluation of unified critical state models. PhD thesis, University of Nottingham, Nottingham, UK; 2004.

65. Khalili N, Habte MA, Valliappan S. A bounding surface plasticity model for cyclic loading of granular soils. *International journal for numerical methods in engineering*. 2005;63(14):1939-1960.

66. Zhou C, Ng CWW. A thermomechanical model for saturated soil at small and large strains. *Can Geotech J*. 2015;52(8):1101-1110.

67. Hu N. On Fabric Tensor-based Constitutive Modelling of Granular Materials: Theory and Numerical Implementation. PhD thesis, University of Nottingham, Nottingham, UK; 2015.

68. Bishop RF, Hill R, Mott NF. The theory of indentation and hardness tests. *Proceedings of Physics Society*. 1945;57:147-159.

69. Mo PQ, Marshall AM, Yu HS. Centrifuge modelling of cone penetration tests in layered soils. *Géotechnique*. 2015;65(6):468-481.

70. Randolph MF, Dolwin J, Beck R. Design of driven piles in sand. *Géotechnique*. 1994;44(3):427–448.

71. Ladanyi B, Johnston GH. Behaviour of circular footings and plate anchors embedded in permafrost. *Can Geotech J*. 1974;11:531-553.

72. Vesic AS. Design of pile foundations. National Cooperation Highway Research Program, Washington, DC; 1977.

73. Yu HS. Discussion on: singular plastic fields in steady penetration of a rigid cone. *J Appl Mech ASME*. 1993;60:1061-1062.

74. van den Berg P. Analysis of soil penetration. PhD thesis, Delft University of Technology; 1994.

75. Lu Q. A numerical study of penetration resistance in clay. PhD Thesis, University of Western Australia; 2004.

76. Robertson PK. Soil classification using the cone penetration test. *Can Geotech J*. 1990;27(1):151-158.

77. Mayne PW. In situ determination of clay stress history by piezocone. *Predictive Soil Mechanics*. 1993, pp. 483-495 (Thomas Telford: London).

78. Mayne, PW. Cone Penetration Testing State-of-Practice. NCHRP Project 20-05, 2007, Topic 37-14.

79. Jamiolkowski M, Ladd CC, Germaine JT, Lanellotta R. New developments in field and laboratory testing of soils. *Theme Lecture, Proc. 11th Int. Conf. on Soil Mechanics and Foundation Engineering*. San Francisco., 1985, pp. 57-156.

80. Ladd CC. Stability Evaluation during Staged Construction. The 22nd Terzaghi Lecture, *Journal of Geotechnical Engineering*. 1991;117(4):540-615.

81. Ladd CC, DeGroot DJ. Recommended Practice for Soft Ground Site Characterization. *Soil & Rock America (Proc. 12th Pan American Conf., MIT)*, Verlag Glückauf, Essen, 2003, pp. 3-57.

82. Durgunoglu HT, Mitchell JK. Static penetration resistance of soils. *Proceedings of the ASCE Specialty Conference on In-Situ Measurements of Soil Properties*, 1975, Vol. 1, pp. 151-189.

83. Been K, Jefferies MG. A state parameter for sands. *Géotechnique*. 1985;35(2):99-112.

84. Been K, Crooks JHA, Becker DE, Jefferies MG. The cone penetration test in sands: I, state parameter interpretation. *Géotechnique*. 1986;36(2):239-249.

85. Been K, Crooks JHA, Becker DE, Jefferies MG. The cone penetration test in sands: II, general inference of state. *Géotechnique*. 1987;37(3):285-299.

86. Yu HS. State parameter from self-boring pressuremeter tests in sand. *J Geotech Engng ASCE*. 1994;120(12):2118-2135.

87. Schnaid F, Yu HS. Interpretation of the seismic cone test in granular soils. *Géotechnique*, 2007;57(3):265-272.

88. Huang AB, Chuang SY. Correlating Cyclic Strength with Fines Contents through State Parameters. *Soils and Foundations*, 2011;51(6):991-1001.

89. Schanz T, Vermeer PA, Bonnier PG. The hardening soil model: formulation and verification. *Proceedings of the beyond 2000 in computational geotechnics: 10 years of PLAXIS international*. Rotterdam (The Netherlands): Balkema, 1999, 281-96.

90. Randolph MF. Characterisation of soft sediments for offshore applications. *Proc., Int. Conf. Geotechnical Geophysical Site Characterization*, ISC-2, Millpress, The Netherlands, 2004, 209-232.

91. DeJong JT, Randolph M. Influence of partial consolidation during cone penetration on estimated soil behavior type and pore pressure dissipation measurements. *J Geotech Geoenviron Eng*. 2012;138(7):777-788.

92. Mahmoodzadeh H, Randolph M. Penetrometer Testing: effect of partial consolidation on subsequent dissipation response. *J Geotech Geoenviron Eng*. 2014;140(6):1-12.

93. Yu HS. Plasticity and Geotechnics. Springer; 2006.

94. Ceccato F, Beuth L, Simonini P. Analysis of Piezocone Penetration under Different Drainage Conditions with the Two-Phase Material Point Method. *J Geotech Geoenviron Eng*. 2016;142(12):1-15.

95. Carter JP, Randolph MF, Wroth CP. Stress and pore pressure changes in clay during and after the expansion of a cylindrical cavity. *Int J Numer Anal Methods Geomech*. 1979;3:305-322.

96. Randolph MF, Carter JP, Wroth CP. Driven Piles in Clay - the Effects of Installation and Subsequent Consolidation. *Géotechnique*. 1979;29(4):361-393.

97. Teh CI, Houlsby GT. An analytical study of the cone penetration test in Clay. *Géotechnique*. 1991;41(1):17-34.

98. Li L, Li JP, Sun DA, Gong WB. Analysis of Time-Dependent Bearing Capacity of a Driven Pile in Clayey Soils by Total Stress Method. *International Journal of Geomechanics*. 2017;17(7):04016156.

99. Mitchell JK. Fundamentals of soil behavior. Wiley, New York; 1976.

100. Burns SE, Mayne PW. Monotonic and Dilatory Pore Pressure Decay during Piezocone Tests. *Can. Geotech. J*. 1998;35(6):1063-1073.

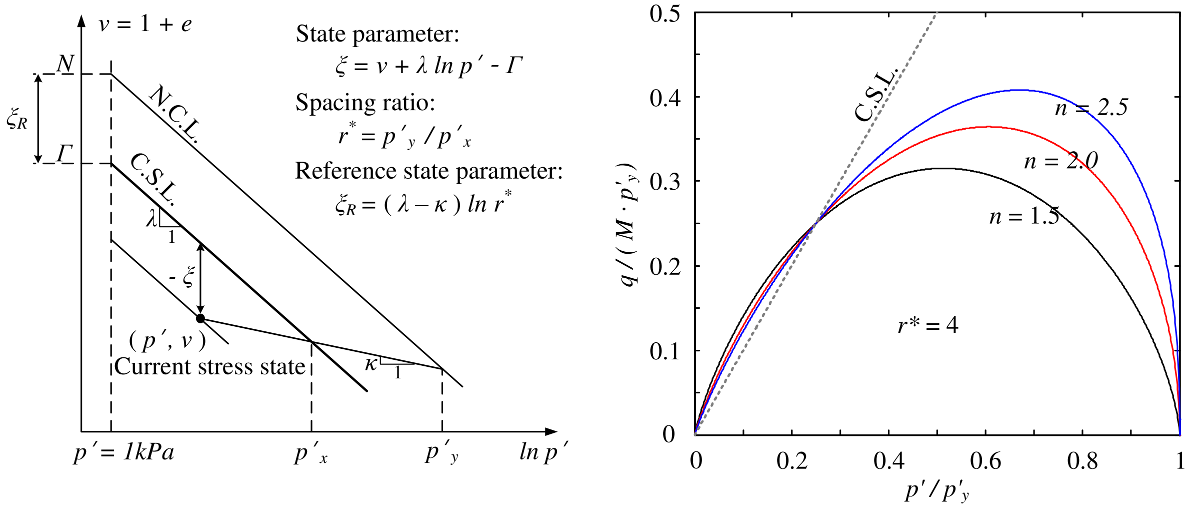

(a) Schematic of state parameter

(b) State boundary surfaces normalised by preconsolidation pressure

FIGURE 1 The illustrations of the unified state parameter model for clay and sand (CASM): (a) state parameter; (b) state boundary surfaces

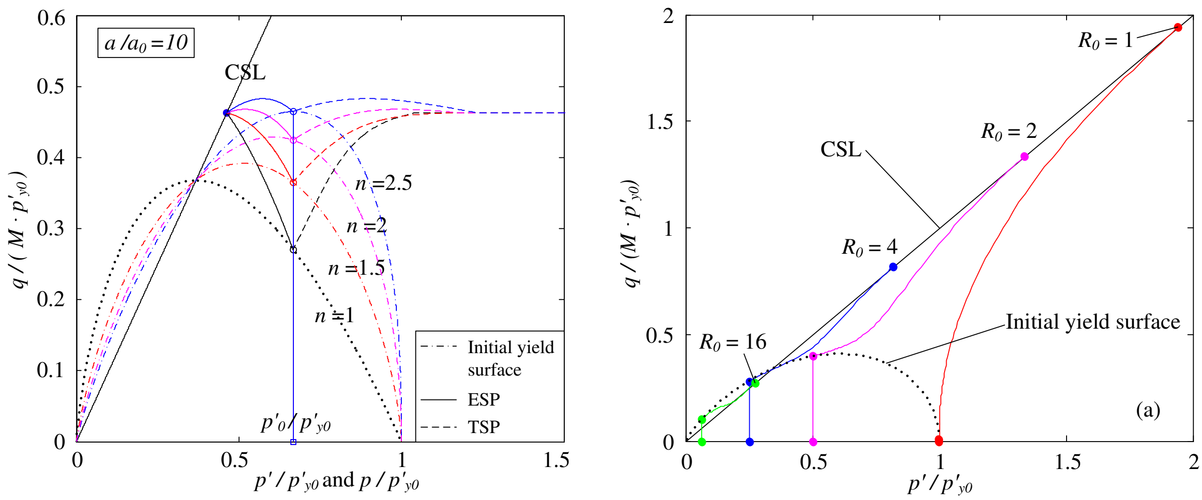

(a) Stress paths at cavity wall for R_0=1.5 (Undrained Expansion)

(b) Stress paths at cavity wall with variation of R_0 (Drained Expansion)

FIGURE 2 Stress paths for soil at the cavity wall: (a) undrained expansion [after Mo and Yu[46]]; (b) drained expansion [after Mo and Yu[53]]

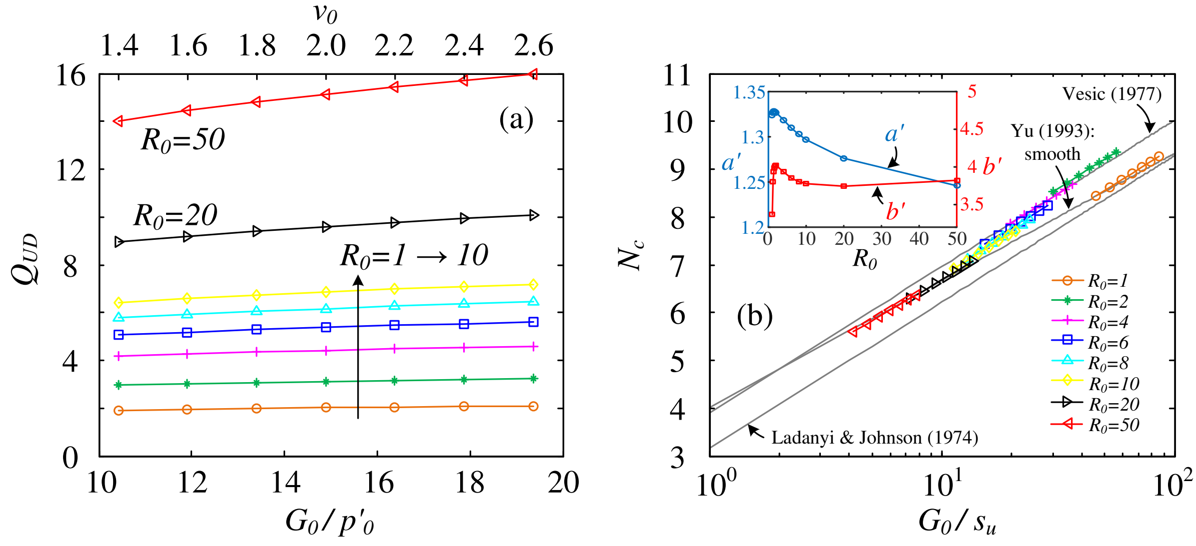

FIGURE 3 Variations of G_0 and R_0 on: (a) the normalised cone tip resistance Q_{UD}; (b) the cone factor under a undrained condition

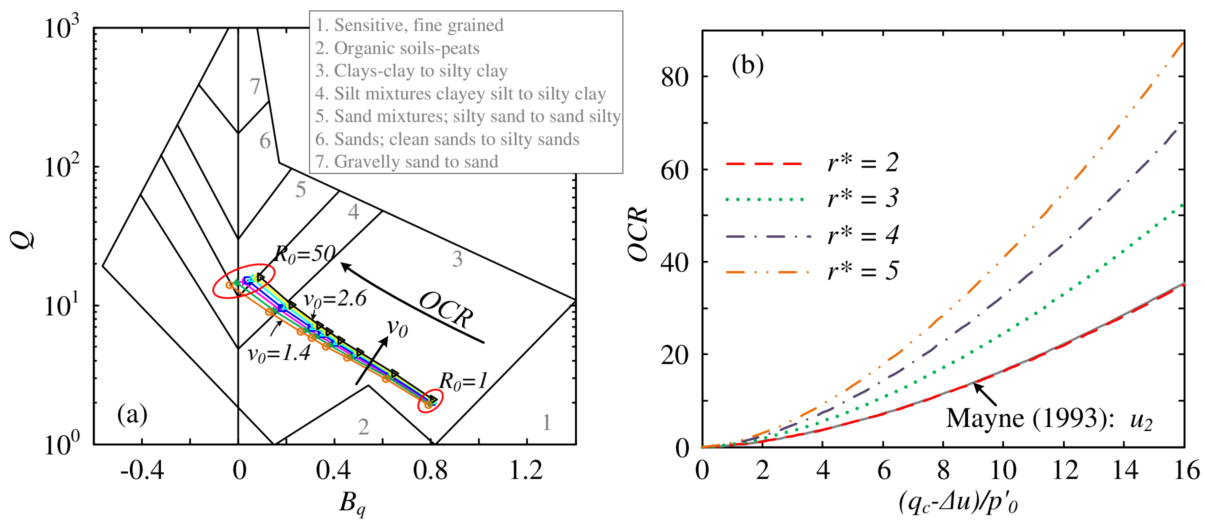

FIGURE 4 Prediction of CPTu data using undrained cavity expansion: (a) the SBT chart; (b) OCR

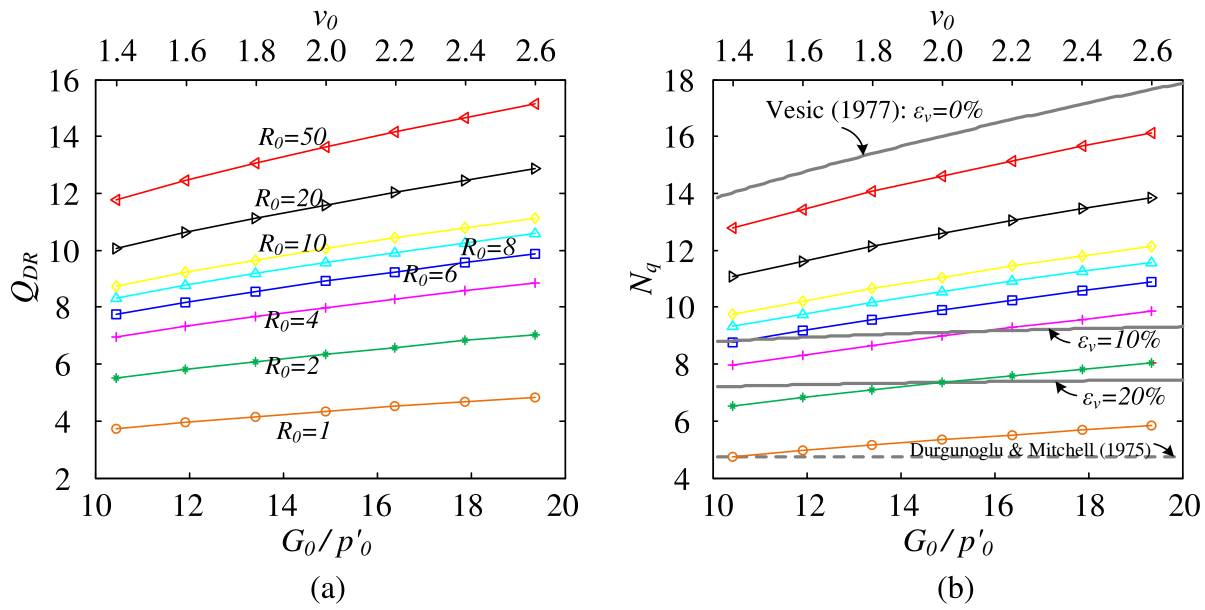

FIGURE 5 Variations of G_0 and R_0 on: (a) the normalised cone tip resistance Q_{DR}; (b) the cone factor under a drained condition

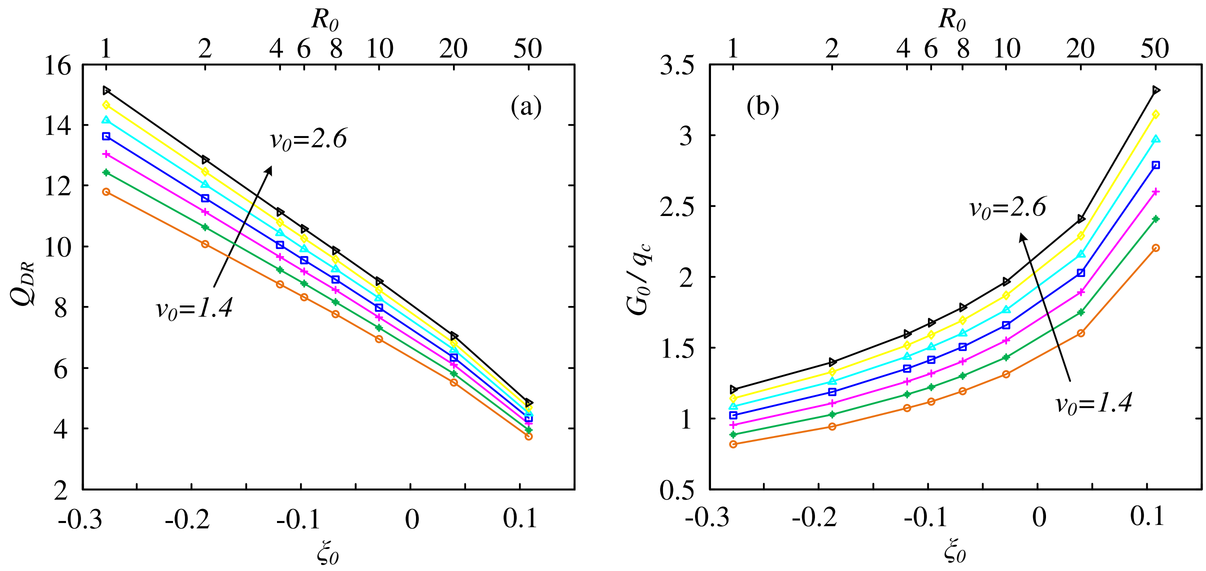

FIGURE 6 Effects of the initial state parameter ξ_0 on: (a) the normalised penetration resistance Q_{DR}; (b) G_0/q_c

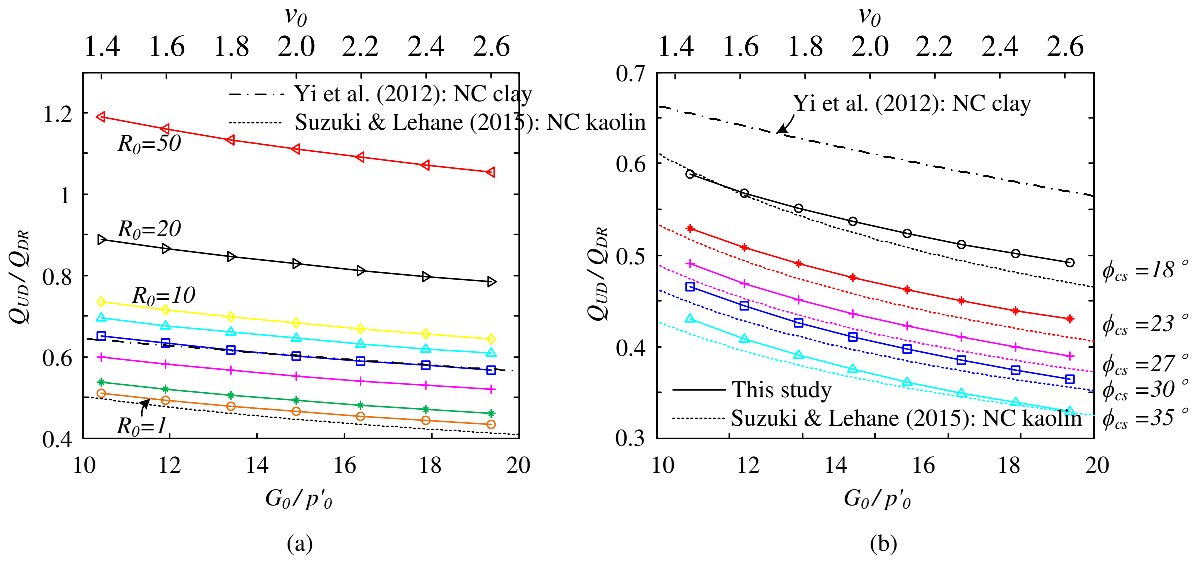

FIGURE 7 Decrease of the undrained-drained resistance ratio against the normalised stiffness with variation of: (a) R_0; (b) ϕ_{cs}

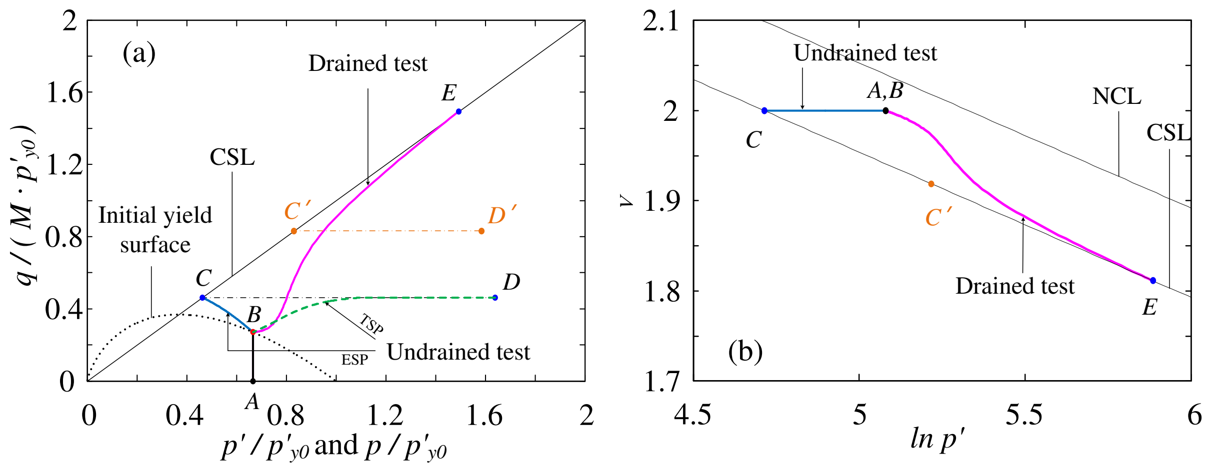

FIGURE 8 Stress paths under various drainage conditions in: (a) $p'/p'_{y0} - q/\left(M \cdot p'_{y0}\right)$ space; (b) $\ln p' - \upsilon$ space

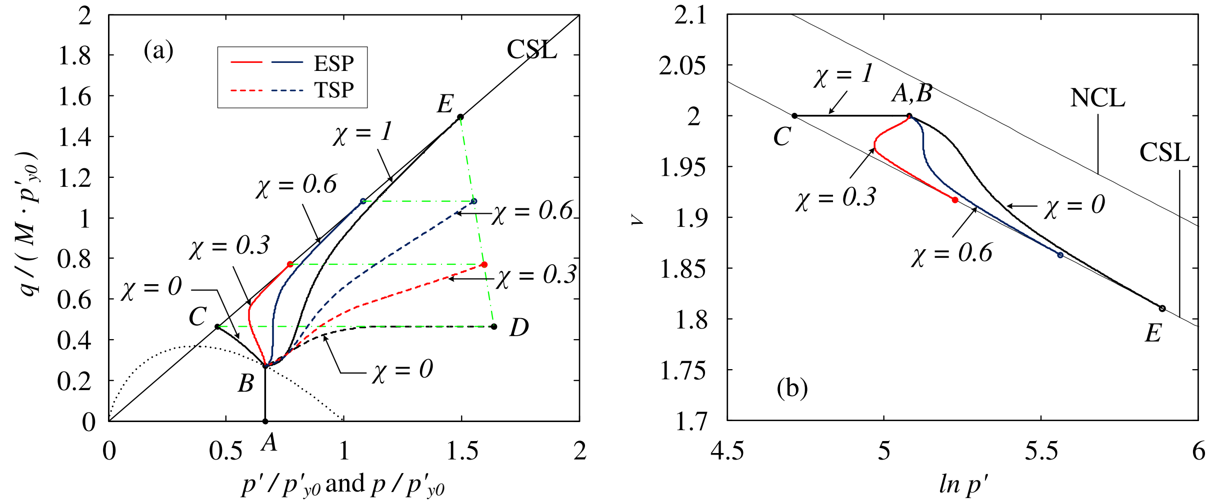

FIGURE 9 Stress paths for soil at the cavity wall with drainage index $\chi = 0, 0.3, 0.6, 1$: (a) $p'/p'_{y0} - q/\left(M \cdot p'_{y0}\right)$ space; (b) $\ln p' - \upsilon$ space

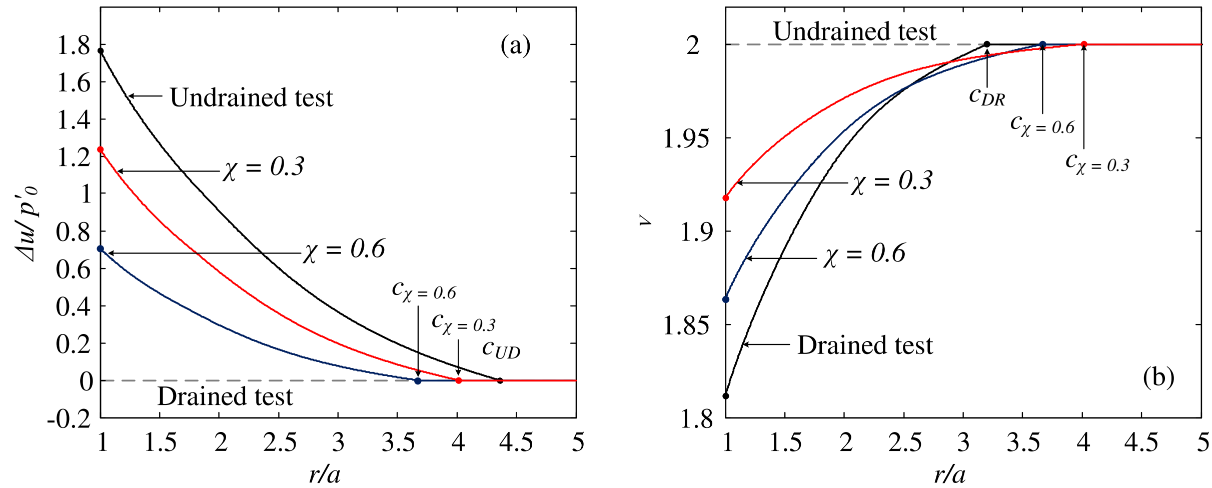

FIGURE 10 Distributions of (a) excess pore pressure and (b) specific volume

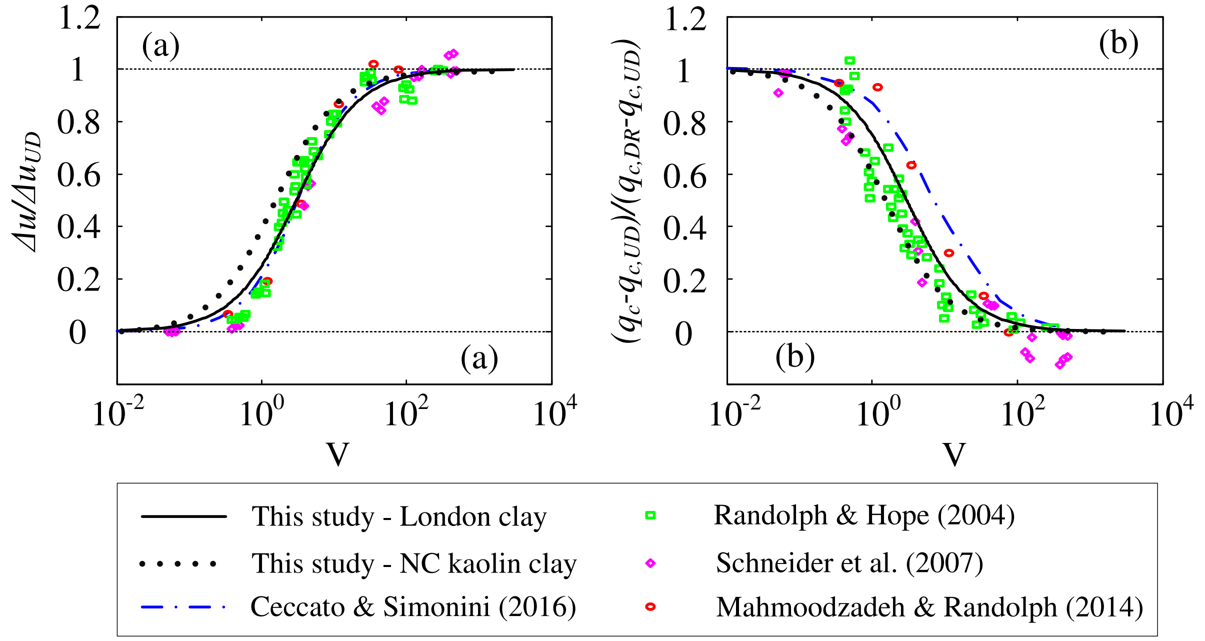

FIGURE 11 Predictions of cone penetration tests at various penetration velocity: (a) excess pore pressure; (b) penetration resistance ratio

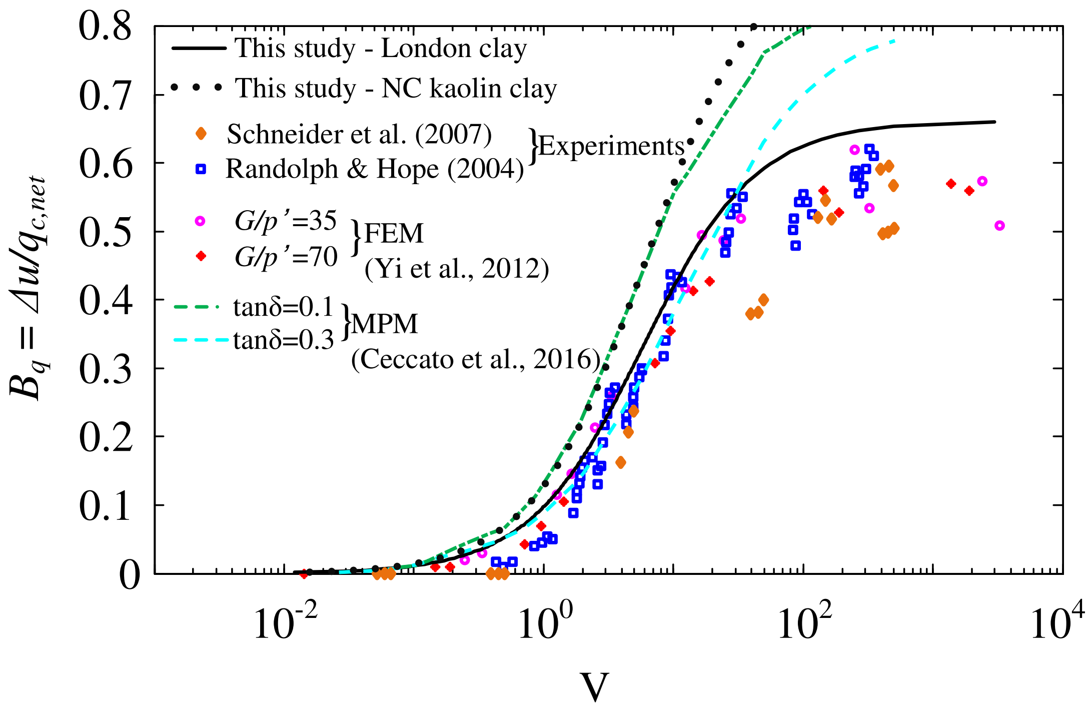

FIGURE 12 Prediction of normalised pore pressure parameter B_q against normalised penetration velocity

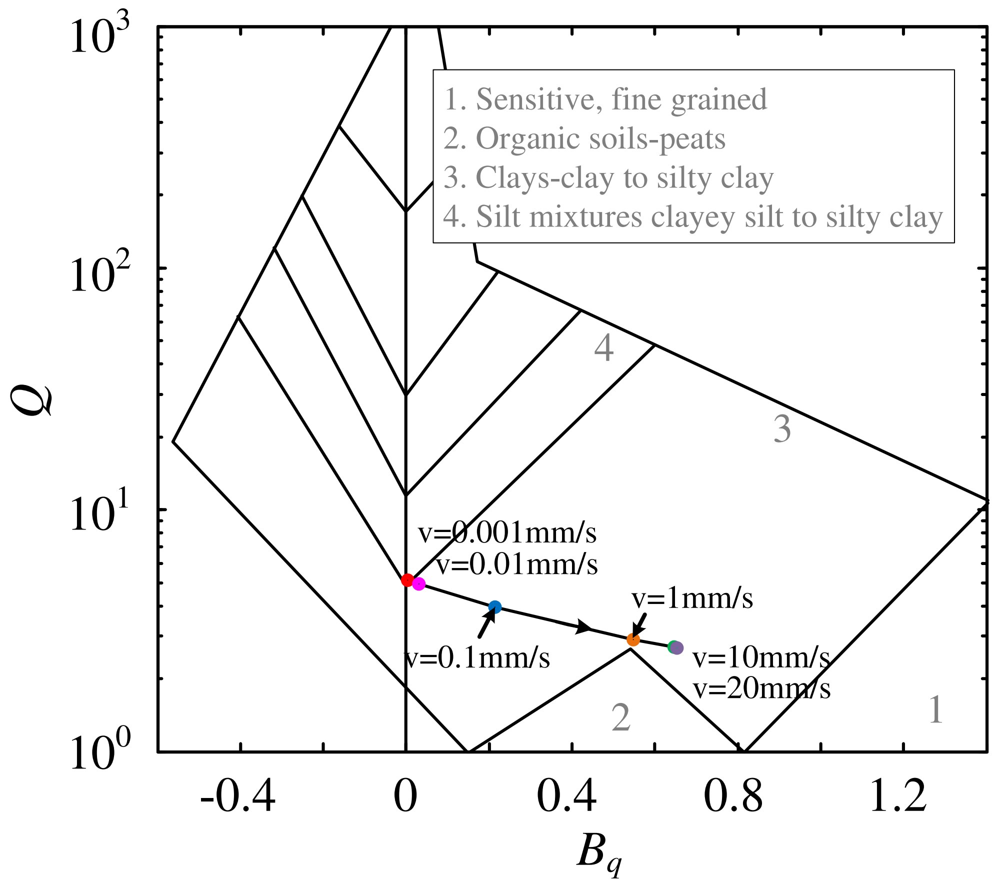

FIGURE 13 CPTu data in London clay on the SBT chart with variation of penetration velocity

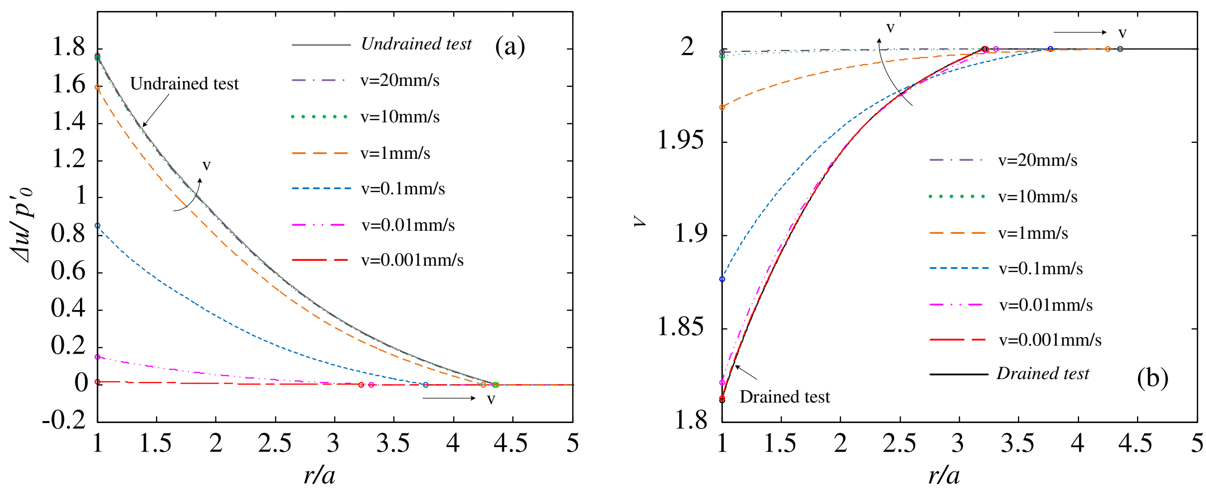

FIGURE 14 Distributions of (a) excess pore pressure, and (b) specific volume, with variation of penetration velocity for London clay

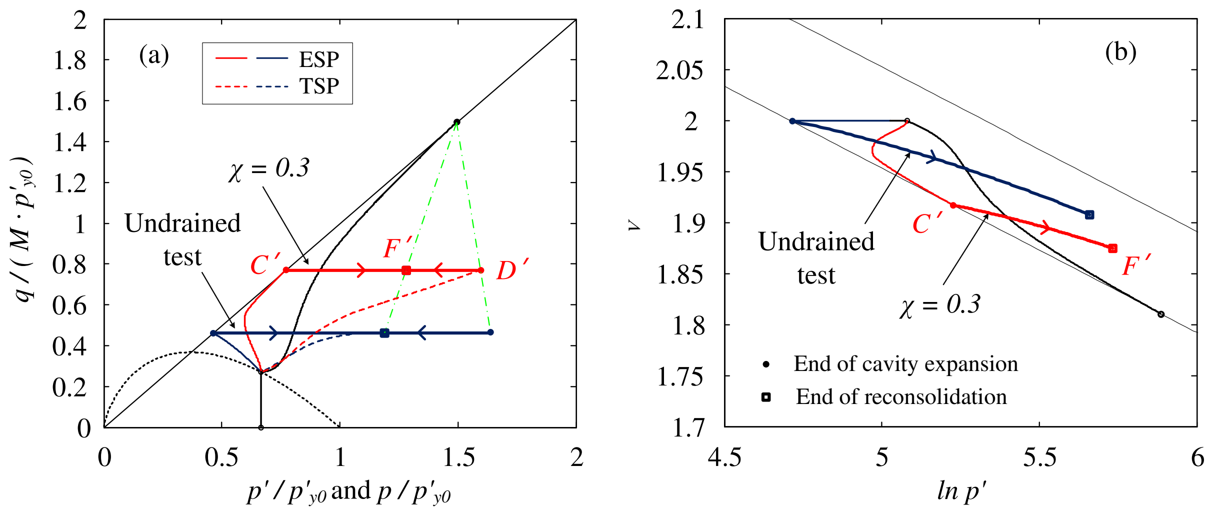

FIGURE 15 Stress paths of reconsolidation after penetration in: (a) $p'/p'_{y0} - q/\left(M \cdot p'_{y0}\right)$ space; (b) $\ln p' - \upsilon$ space

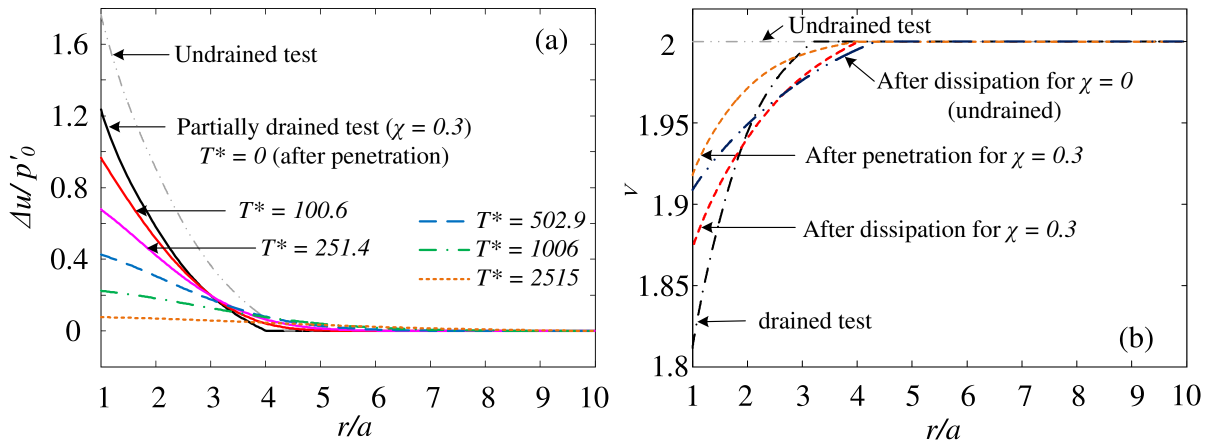

FIGURE 16 Distributions of (a) excess pore pressure, and (b) specific volume, before and after reconsolidation

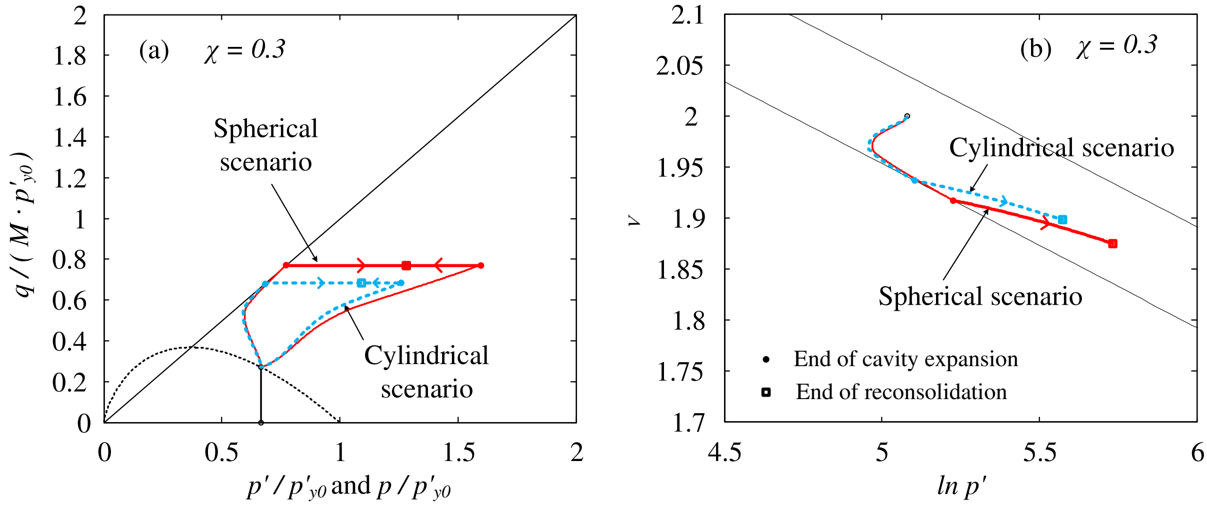

FIGURE 17 Stress paths for both spherical and cylindrical scenarios in: (a) $p'/p'_{y0} - q/\left(M \cdot p'_{y0}\right)$ space; (b) $\ln p' - v$ space

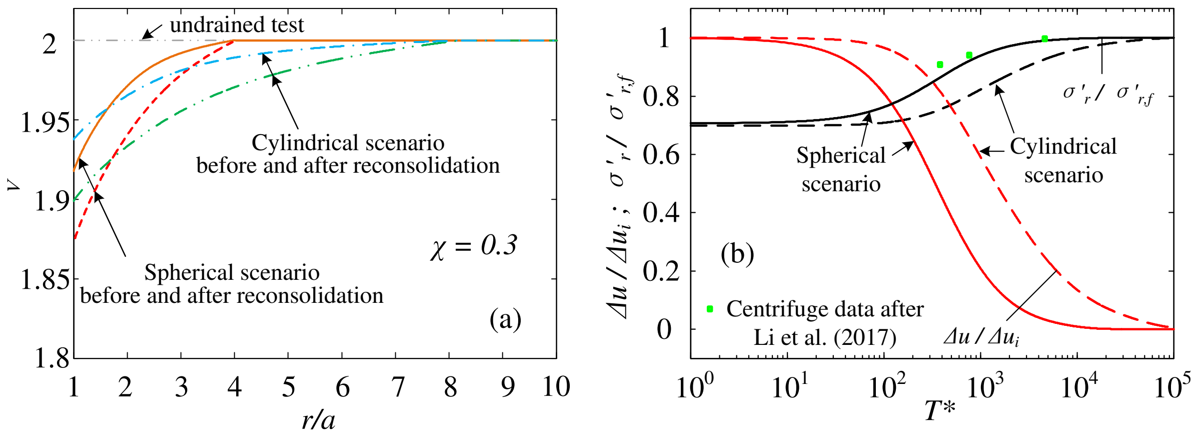

FIGURE 18 Comparisons of spherical and cylindrical scenarios: (a) distributions of specific volume before and after reconsolidation; (b) changes of pore pressure and radial stress with normalised reconsolidation time

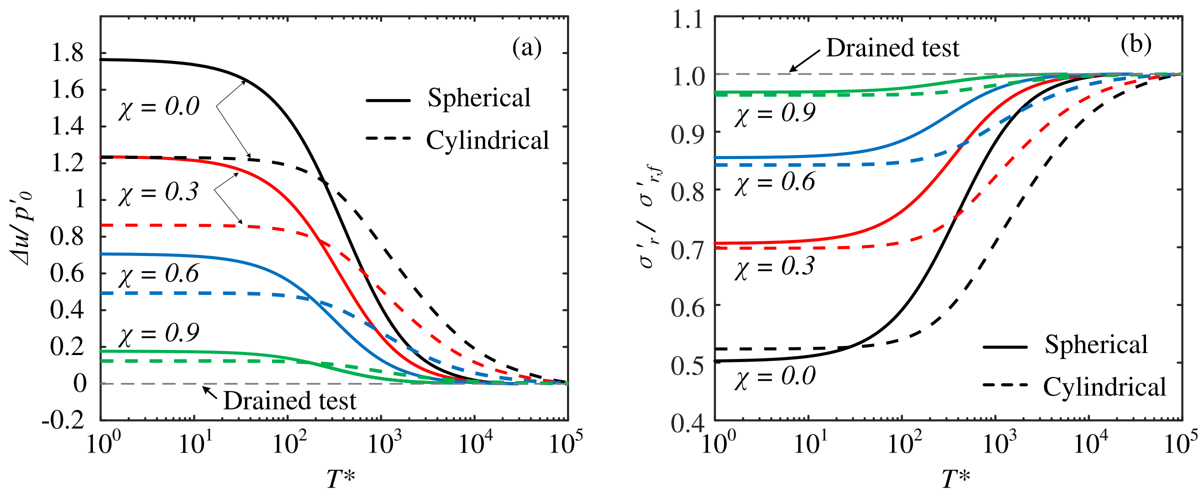

FIGURE 19 Changes of pore pressure and radial stress with different values of drainage index for both spherical and cylindrical scenarios: (a) normalized excess pore pressure and (b) normalized radial stress

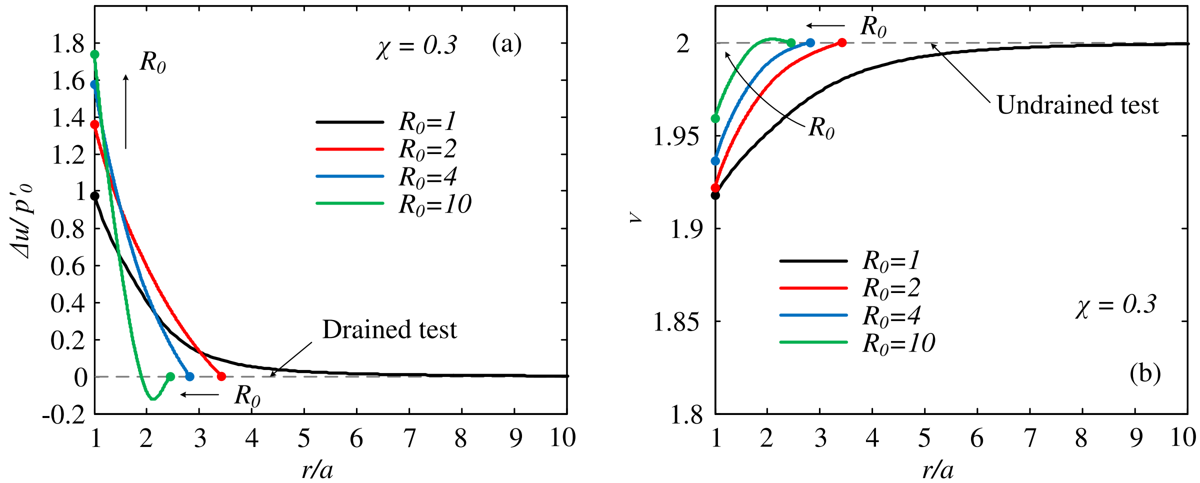

FIGURE 20 Distributions of (a) excess pore pressure and (b) specific volume, after cavity expansion with variation of R_0 for $\chi = 0.3$

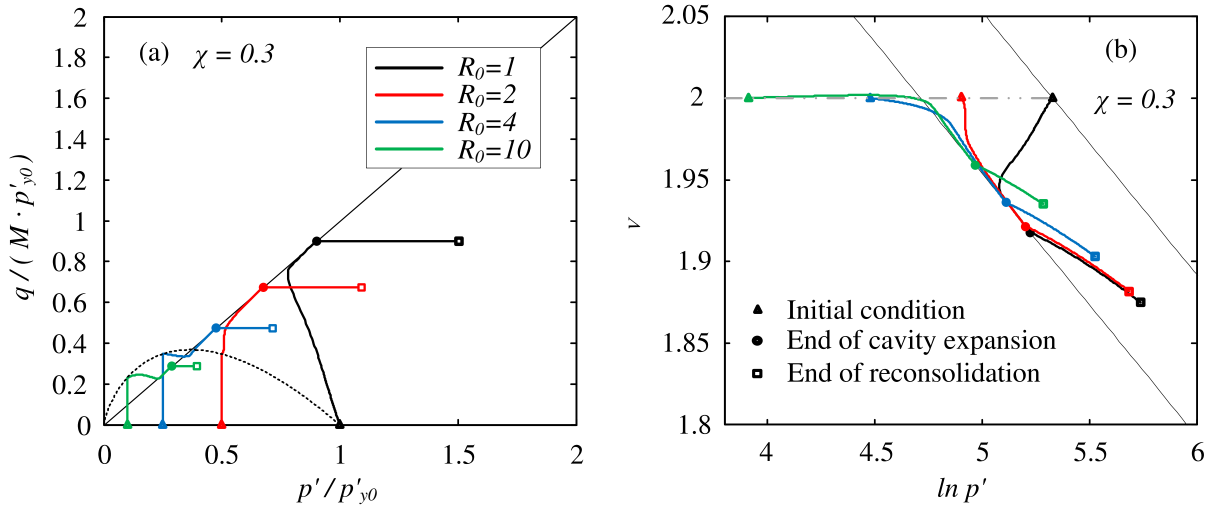

FIGURE 21 Stress paths of cavity expansion and reconsolidation in: (a) $p'/p'_{y0} - q/\left(M \cdot p'_{y0}\right)$ space; (b) $\ln p' - \upsilon$ space, with variation of R_0 for $\chi = 0.3$

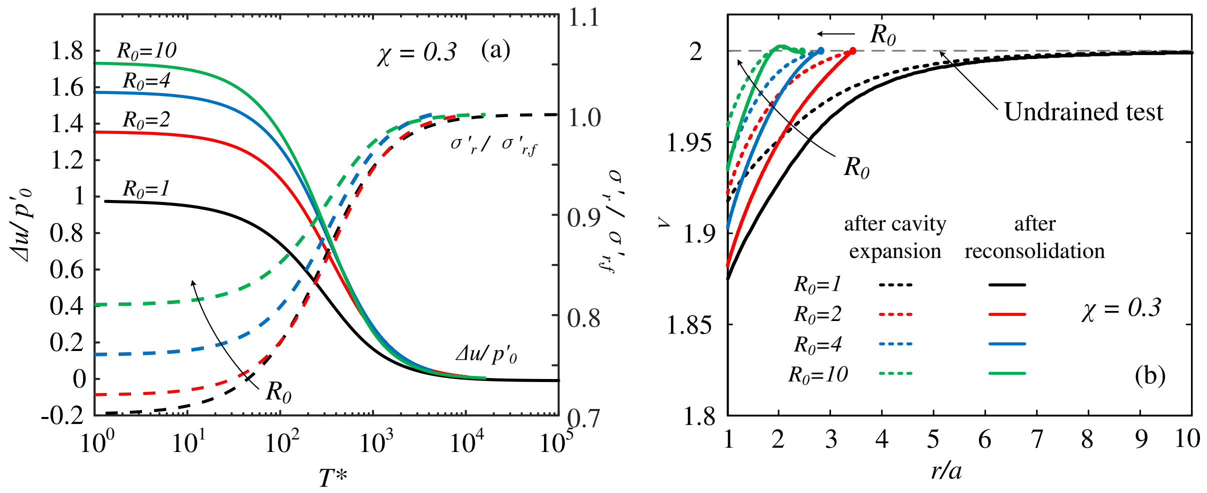

FIGURE 22 Changes of pore pressure and specific volume during reconsolidation with variation of R_0 for $\chi = 0.3$: (a) normalized excess pore pressure dissipation and (b) distributions of specific volume